# Advanced Processing and Characterization of Al-Based Composites Containing $Al_3X$ Intermetallics Platelets

2011

Shimaa El-Hadad

名古屋工業大学博士論文
甲第764号(課程修了による)
平成２３年３月２３日授与

# Advanced Processing and Characterization of Al-Based Composites Containing $Al_3X$ Intermetallics Platelets

by

**Shimaa El-Hadad**

**Thesis for Ph. D. degree of engineering**

**Department of Engineering Physics, Electronics and Mechanics,**
**Graduate School of Engineering,**
**Nagoya Institute of Technology,**
**Nagoya, Japan.**

**2011**

# Advanced Processing and Characterization of Al-Based Composites Containing $Al_3X$ Intermetallics Platelets

Thesis submitted to
Graduate School of Engineering,
Nagoya Institute of Technology.
Doctor degree of engineering.

by

**Shimaa El-Hadad**

Supervisors

**Prof. Yoshimi Watanabe**
**Prof. Hisashi Sato**

Department of Engineering Physics, Electronics and Mechanics

**2011**

To whom it may concern

We hereby certify that this is a typical copy of the original doctor thesis of

**Mrs. Shimaa El-Hadad**

Thesis title

**Advanced Processing and Characterization of Al-Based Composites Containing $Al_3X$ Intermetallics Platelets**

Official seal of the institute

President of Nagoya Institute of Technology

**To my parents, my husband**
**and my little kids**

# Declaration of Originality

I hereby declare that the research recorded in this thesis and the thesis itself was accomplished and originated entirely by myself in the Graduate School of Engineering at Nagoya Institute of Technology.

Shimaa El-Hadad

## Abstract

Aluminum rich intermetallics and alloys are important for their tribological applications and scientifically interesting for their complex structures. Aluminum based intermetallics compounds boast high-strength/high temperature and they are oxidation resistant compounds. Such attractive characteristics make tri-aluminides $Al_3X$ (X= Ti, Zr, V, etc.) potential candidates for high temperature structural applications. However, brittleness at low temperatures has limited the application of these alloys.

Among these alloys, Al-5 mass% Ti and Al-5 mass% Zr alloys were chosen as master alloys in the current study. Some advanced processing techniques were applied to make use of these alloys containing brittle $Al_3X$ particles without changing their crystal structures. Al-$Al_3Zr$ and Al-$Al_3Ti$ alloys were severely deformed via equal channel angular pressing (ECAP). The ECAPed samples showed a notable decrease in the size of the $Al_3X$ platelets and an increased tendency to align parallel to the deformation axis with increasing the number of passes. Some anisotropy in the mechanical properties of the ECAPed specimens was observed at 4 passes of deformation; however, this anisotropy became negligible with increasing the number of deformation passes.

In the tribological applications where the wear resistant surface is an essential requirement, fragmentation of $Al_3X$ particles which act as load supporting elements is not recommended. Therefore, another technique that overcomes the brittleness of $Al_3X$ particles and keeps their good wear resistance as well has been applied. Al-$Al_3Ti$ and Al-$Al_3Zr$ functionally graded materials (FGMs) were fabricated by the centrifugal casting method (CCM). Microstructural observation along the centrifugal force direction showed that $Al_3X$ platelet particles are almost oriented normal to the applied centrifugal force direction. Volume fraction of $Al_3X$ particles increases close to the ring surface. Moreover, this distribution range of $Al_3X$ particles becomes broader with decreasing the applied centrifugal force. The wear anisotropy of the fabricated Al-$Al_3X$ FGMs was strongly influenced by the platelet particles orientation at the test position. Investigating both of the worn surface morphology and the sub-worn surface layer showed that plastic deformation induced by wear is the dominant

mechanism during the wear process of Al-$Al_3X$ FGM samples.

After fabricating the FGMs, the effect of processing temperature on the microstructure and mechanical properties of Al-$Al_3Ti$ FGMs fabricated by centrifugal solid-particle method (CSPM) and *in-situ* method (CISM) was evaluated. CISM showed a slower compositional gradient and larger $Al_3Ti$ particle size than that of CSPM-FGMs. The higher temperature in the CISM resulted in higher degree of $Al_3Ti$ platelets orientation in the outer surface of the samples compared to those of CSPM-FGMs. The CSPM samples showed better wear resistance than those of CISM.

In the last part, Al-$Al_3Ti$ FGMs were fabricated by a novel reaction centrifugal mixed-powder method (RCMPM) under different temperatures. Effect of RCMPM processing temperature on the formation of $Al_3Ti$ intermetallics, its morphology and its distribution in the fabricated Al-$Al_3Ti$ FGMs was investigated. Fine granular $Al_3Ti$ were observed at relatively lower processing temperature while the known coarse platelet-like particles of $Al_3Ti$ could be achieved at higher casting temperatures. Moreover, $Ti_3Al$ intermetallics compound and unreacted Ti phases are found for the sample fabricated at lower processing temperature. In addition, distribution of $Al_3Ti$ intermetallics size and their volume fraction showed a significant change when the Al-$Al_3Ti$ FGMs processed at different temperatures relative to the liquidus

In summary, the process to be applied on Al-based alloys containing platelet intermetallics should be carefully selected. If the application requires considerably homogeneous structures with finely dispersed reinforcements, then SPD is the recommended choice. On the other hand, if the processed part will be used for tribological applications where the wear resistant surface is the essential demand, FGMs is the suitable method.

## Acknowledgments

It is almost three years that I have spent in the group of Prof. Watanabe laboratory, working on the research presented in this thesis. I would like to say that working in this group was always pleasant and stimulating. I am really indebted to many colleagues and friends for their kind help and would like to take this opportunity to thank specially those who have played a significant role in helping me bring this work to fruition.

First I would like to thank the God, who gave me sufficient energy and courage to carry out this research and complete this thesis. My much gratitude is owed to Profs. Yoshimi Watanabe and Hisashi Sato for their continuous guidance and support. Thanks are due to my colleges, Tabushi, Inaguma, Kubuta and Furukawa for their help during the experiments. I am also grateful to Prof. Miura, Ms. Yamada, Ms. Asai and all the laboratory members for their continuous guidance during my stay in Japan

I am thankful to Profs. Adel Nofal and Mohamed Waly (Central Metallurgical Research and Development Institute, Egypt) for helping me to obtain the scholarship provided by the Egyptian government to study in Japan. Further, the support from "Grant-in-Aid for Scientific Research on Priority Areas (19025005)" and "Tokai Region Nanotechnology Manufacturing Cluster in Knowledge Cluster Initiative" by the Ministry of Education, Culture, Sports, Science and Technology of Japan is also acknowledged.

Finally, my deep thanks are to my husband for his moral help and encouragement during my study in Japan.

# Table of Contents

# Chapter 1
# Introduction and Literature Survey

## 1.1. Al-Rich Intermetallics in Aluminum Alloys

Aluminum rich intermetallics and alloys are important for their tribological applications and scientifically interesting for their complex structures. Aluminum based intermetallics compounds boast high-strength/high temperature and oxidation resistant compounds [1]. Such attractive characteristics make tri-aluminides $Al_3X$ (X = Ti, Zr, V, Nb, Hf, Ta) potential candidates for high temperature structural applications. However, brittleness at low temperatures has limited the application of these materials. [2]

Among Al-$Al_3X$ type alloys, Al-$Al_3Ti$ and Al-$Al_3Zr$ alloys containing platelets intermetallics have been chosen as master alloys in the current work. The partial phase diagrams of these alloys are shown in Fig.1.1 and Fig.1.2 [3] wherein the master alloys used in this study are indicated by dotted lines. Both of $Al_3Ti$ and $Al_3Zr$ are characterized by their good lattice matching with the Al matrix, which results in low interfacial energy and thus low driving force for particles coarsening [4]. Furthermore, the low diffusivity of those intermetallics in Al strict their growth and provide the needed phase stability for high temperature applications. [4, 5]

From Fig.1.1, the $Al_3Ti$ intermetallics compound solidifies through a peritectic reaction. This intermetallics phase crystallize with up to 37 mass% Ti into a tetragonal structure of the $D0_{22}$ type. The $D0_{22}$ structure derives from the $L1_2$ cubic structure as reported earlier [6]. The Al-Zr partial phase diagram, Fig.1.2, shows that $Al_3Zr$ intermetallics are formed through peritectic reaction and congruent melting. This compound in its stable phase has the tetragonal ($D0_{23}$) structure which is also derivative of the $L1_2$ structure. In addition, the $L1_2$ cubic $Al_3Zr$ can form at low temperatures from the supersaturated solid solution and transform to the equilibrium $D0_{23}$ phase at high temperatures [6].

The lack of ductility of those tri-aluminides is attributed to their low crystal symmetry of the tetragonal $D0_{22}$ or $D0_{23}$ structures [7]. That is, they do not have a sufficient number of

equivalent slip systems to satisfy the von-Mises criterion for slip deformation in poly-crystals. In $Al_3X$ intermetallics, the tetragonal $D0_{22}$ or $D0_{23}$ structure is closely related to the cubic $L1_2$ structure that has five independent slip systems. Structural isotropy is expected to improve the deformability of the material because the isotropy increases the variants of active slip systems for dislocation motions. Thus, the stabilization of the $L1_2$ structure is of great interest for practical purposes as well as for the comprehensive understanding of stabilization. [2, 8-11].

A number of studies have recently been devoted to determine the effect of the presence of third elements (Cr, Mn, Fe, Co, Ni, Cu, Zn, Ag and Pd) in the stabilization of the $L1_2$ structure [8]. Since the $L1_2$ structure has more slip systems, the ductility of $Al_3Ti$ and $Al_3Zr$ is improved. However, neither the origin of this effect nor the influence of atom-species quantities is fully understood yet.

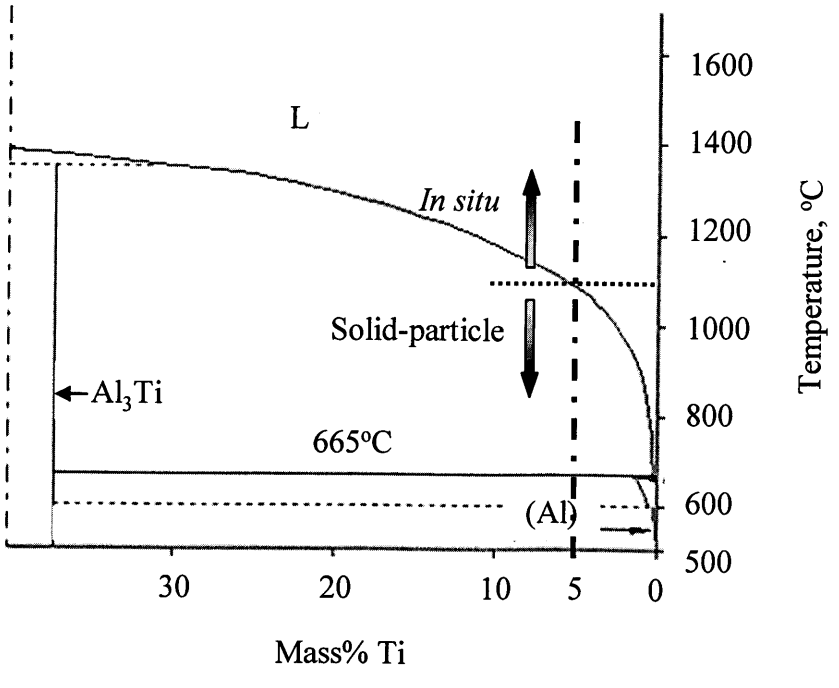


**Fig.1.1. Al-Ti phase diagram. [3]**

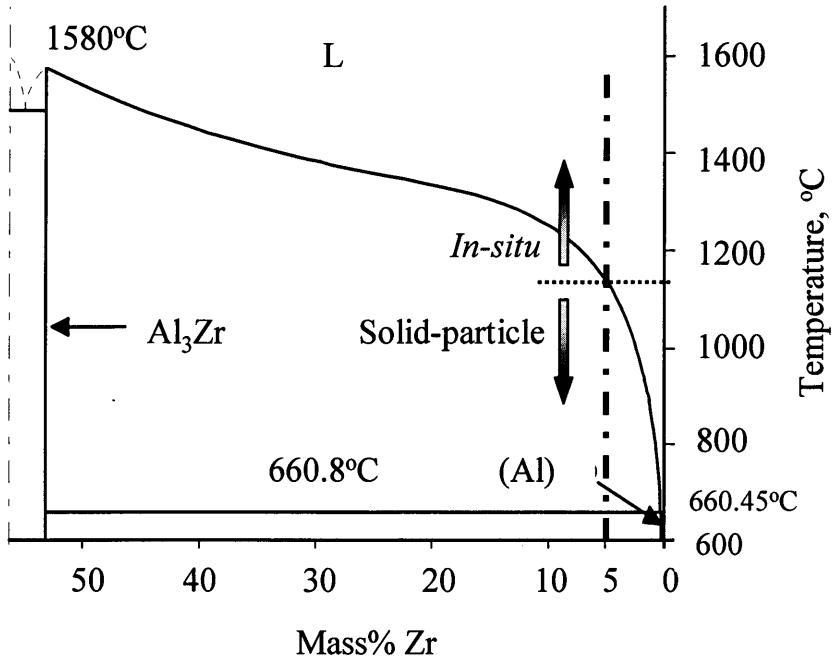


**Fig.1.2. Al-Zr phase diagram. [3]**

## 1.2. Advanced Processing of Al-$Al_3X$ Alloys

Recently, some of the advanced processing techniques are applied to make use of Al-$Al_3X$ alloys containing brittle $Al_3X$ particles without changing their crystal structures. Of these techniques, severe plastic deformation (SPD) of Al-$Al_3X$ alloys by which the brittle $Al_3X$ platelet particles can be fragmented and thus better mechanical properties can be obtained [12, 13]. Processing by SPD refers to various experimental procedures of metal forming that may be used to impose very high strains on materials leading to ultra fine grained (UFG) structures. A unique feature of SPD processing is that the high strain is imposed without any significant change in the overall dimensions of the work piece. Another feature is that using special tool geometries that prevent free flow of the material and thereby produce a significant hydrostatic pressure retains the shape [12, 13]. The presence of this hydrostatic pressure is essential for achieving high strains and introducing the high densities of lattice defects necessary for exceptional grain refinement [14].

The SPD methods are demonstrated in such techniques as equal channel angular extrusion or pressing (ECAE or ECAP) [15, 16], high pressure torsion (HPT) [17], twist extrusion (TE) [18], friction stir processing (FSP) [19], and multi directional forging (MDF), also known as multiaxial compression/forging (MAC/F) [20]. In addition, there are several methods of producing sheet metals, such as accumulative roll bonding (ARB) [21] and repeated corrugation and straightening (RCS) [15, 22].

However, in the tribological applications where the wear resistant surface is an essential requirement, fragmentation of $Al_3X$ particles is not recommended. Therefore, another technique that overcomes the brittleness of $Al_3X$ particles and keeps their good wear resistance as well has been proposed [23]. A proper gradient distribution of these coarse intermetallics compounds in a ductile matrix would result in better properties than a homogeneous distribution, based on the concept of functionally graded materials (FGMs) [24-30]. FGMs can be defined as new advanced multifunctional composites where the volume fractions of the reinforcement phase(s) vary in a gradual manner. This is achieved by using reinforcements with different properties, sizes, and shapes, as well as by interchanging the functions of the reinforcement and matrix phases in a continuous manner. The result is a microstructure bearing continuous changes in thermal and mechanical properties at the macroscopic or continuum scale [31-33].

Fig.1.3 shows different ways of particle distributions within the composite and its effect on generic properties. The first way is to distribute the particles homogeneously in order to obtain uniform properties, as shown in Fig. 1.3 (a). The second way is to induce a layer of particles into the matrix, as shown in Fig. 1.3 (b), which results in abrupt discontinuity in the properties. This type of distribution causes localized tension concentration and can be detrimental to the materials resistance [6]. The most recent type is to create a gradual distribution of the second phase particles within the matrix which results in a corresponding graded property, as shown in Fig. 1.3 (c). Several FGM fabrication methods have been proposed, such as chemical vapor deposition, plasma spray technique and various powder metallurgy techniques. However, it has been difficult to produce relatively large FGM components by most fabrication methods [26, 34]. In addition, those methods require relatively

new techniques and expensive fabrication equipment.

Fabrication of FGMs by a centrifugal method (CM) was introduced recently and has attracted a lot of attention due to its unique merits. The selective reinforcement obtained by CM results in high wear resistance of the component surface as well as maintaining high bulk toughness [27, 35]. In particular, Al based FGMs fabricated by the CM showed interesting properties that are not obtained in conventional monolithic materials, such as gradual changes in hardness, wear resistance, Young's modulus, *etc* [36].

In the current study, as SPD process, ECAP was applied to process Al-5 mass% Ti and Al-5 mass% Zr alloys through different processing routes. Fabrication of Al-$Al_3Ti$ FGMs and Al-$Al_3Zr$ FGMs was performed using the CM; different CM techniques were used.

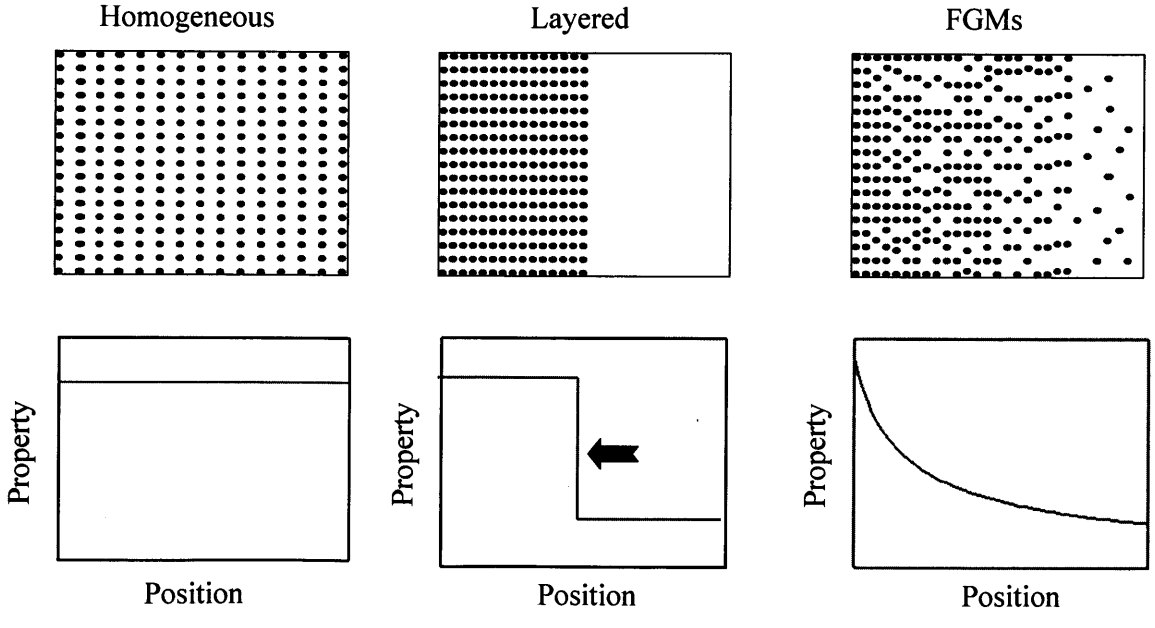


**Fig.1.3. Three types of composite materials, a) homogeneous composite, b) coated or jointed composite, and c) FGMs**

### 1.2.1. Severe Plastic Deformation via ECAP

ECAP is at present the most developed SPD processing technique [13, 16]. As illustrated in Fig.1.4, a rod-shaped billet is pressed; a shear strain is introduced when the billet passes through the point of intersection of the two parts of the channel. Since the cross-sectional dimensions of the billet remain unchanged, the pressings may be repeated to attain exceptionally high strains.

The equivalent strain, $\varepsilon$, introduced in ECAP is determined by a relationship incorporating the angle between the two parts of the channel, $\Phi$, and the angle representing the outer arc of curvature where the two parts of the channel intersect, $\Psi$. The relationship is given by, [13]

$$\varepsilon=(N/\sqrt{3})[2\cot\{(\Phi/2)+(\Psi/2)\}+\Psi \operatorname{cosec}\{(\Phi/2)+(\Psi/2)\}] \quad (1\text{-}1)$$

In practice, different slip systems may be introduced by rotating the billet about its longitudinal axis between each pass and this leads to four basic processing routes: There is no rotation of the billet in route A, rotations by 90° in alternate directions in case of route $B_A$ and in the same direction in route $B_C$. While in route C, the sample is rotated by 180° in route C as shown in Fig. 1.5. When using a die with a channel angle of $\Phi = 90°$, route $B_C$ is generally the most expeditious way to develop an UFG structure consisting of homogeneous and equiaxed grains [12, 37]. The processing routes which will be used in this thesis are A and $B_C$. Route A is defined as unidirectional route in which the strain is accumulated in one direction thus resulting in an anisotropic structure. On the other side, route $B_C$ is a homogeneous ECAP processing route by which a homogeneous structure can be achieved [12].

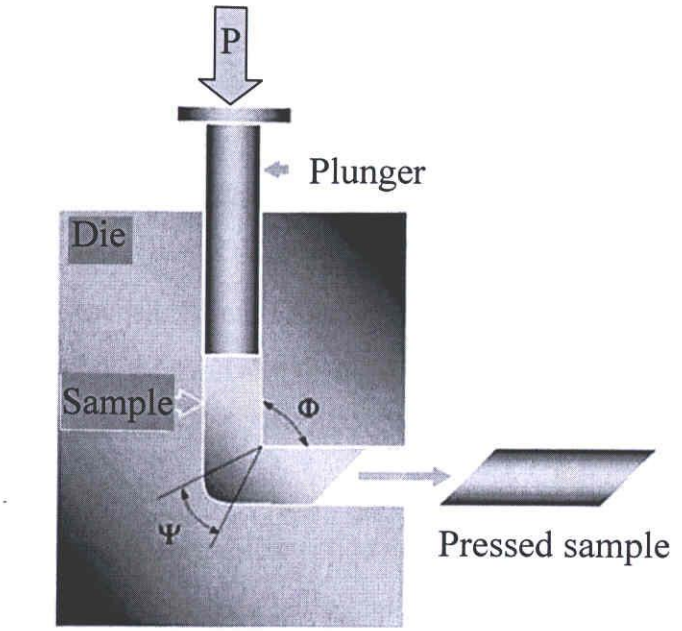


**Fig.1.4. The principle of ECAP [38].**

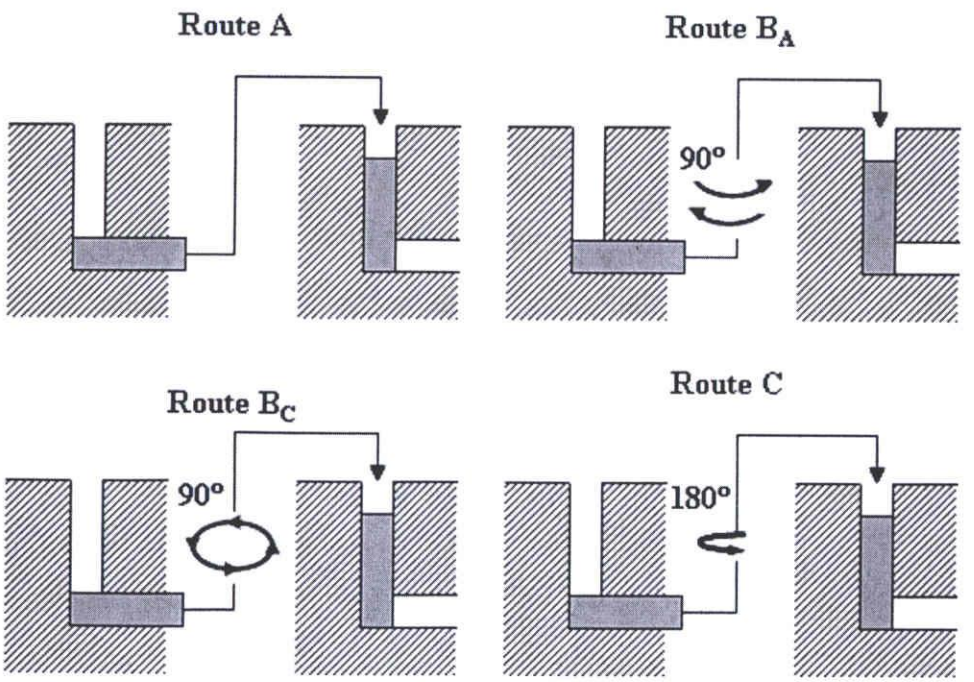


**Fig.1.5. Schematic illustration of ECAP processing routes.**

### 1.2.2. Fabrication of Functionally Graded Materials by Centrifugal Method

Fabrication of FGMs based on mass/heat transport phenomenon includes the self-propagating synthesis and gravity or centrifugal segregation methods as reported by Suresh and Mortensen [34]. Recent studies for Watanabe *et al* [24, 28] on $Al_3Ti$ have suggested that the alternative solution for the poor ductility of $Al_3Ti$ is to disperse the particles in a ductile aluminum matrix. Based on this idea, Al-$Al_3Ti$ FGMs have been developed using the CM [27, 39-41], centrifugal force is applied to a mixture of molten metal and dispersed material, such as ceramic powder or intermetallics compounds, leads to the formation of a desired composition gradient. The gradient is controlled mainly by the difference in density between the matrix and the dispersed material, *G* number (centrifugal force magnitude) and casting temperature.

Fabrication of intermetallic compound-dispersed FGMs by the CM can be classified into two categories based on the relation between the processing temperature and the liquidus temperature of master alloy. If the liquidus temperature of the master alloy is significantly higher than the processing temperature, the dispersed phase remains solid in a liquid matrix during the process. This situation is similar to ceramic-dispersed FGMs, and this method is referred to as a centrifugal solid-particle method (CSPM) [39].

On the other hand, if the liquidus temperature of the master alloy is lower than the processing temperature, centrifugal force can be applied during the solidification of both the dispersed phase and the matrix. This solidification is similar to the production of *in situ* composites using the crystallization phenomena, and this method is, therefore, named as a centrifugal *in-situ* method (CISM). The two FGMs-CM fabrication concepts are illustrated in Fig. 1.6 [42, 43].

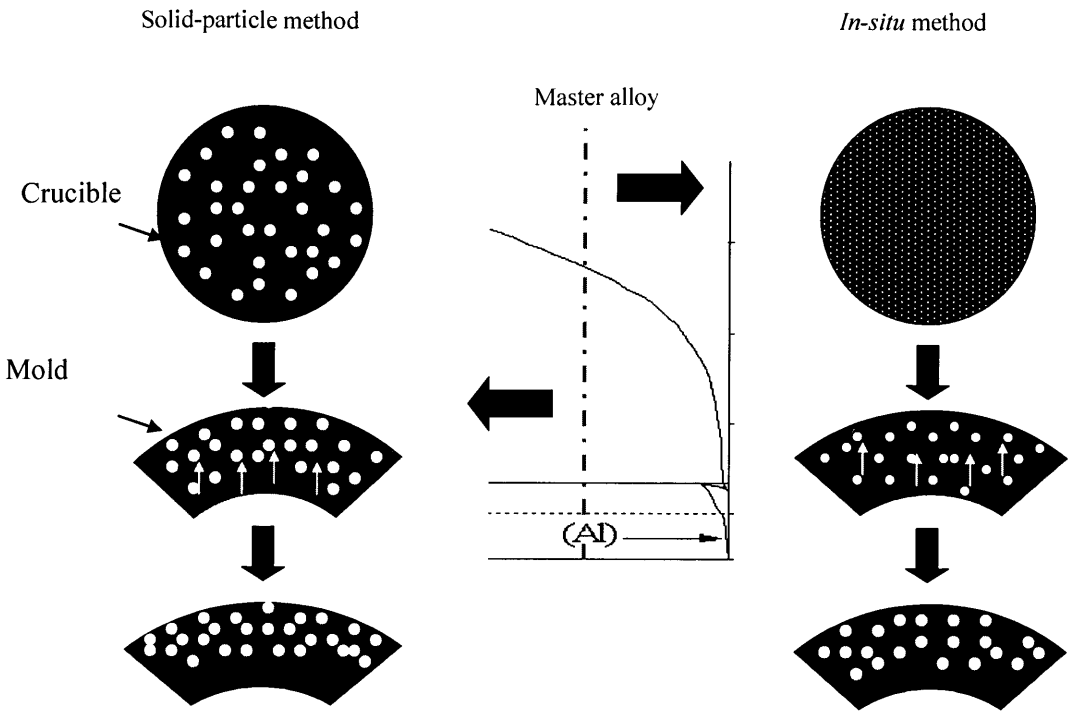


**Fig. 1.6. Schematic illustration of CSPM and CISM.**

Recently, a more practical CM process, the centrifugal mixed-powder method (CMPM) was developed by Watanabe *et al.* [44, 45]. In this method, a powder mixture of dispersion-particles, *B*, and matrix metal particles, *A*, is inserted into a spinning mold. Then, matrix metal ingot, *A*, is melted and poured into the spinning mold with powder mixture *A*+*B*. As a result, the molten matrix metal, *A*, penetrates into the space between the particles by the pressure due to the centrifugal force. At the same time, powder of matrix metal, *A*, is melted by the heat from molten matrix poured from crucible. Finally, an FGM ring with dispersion-particles, *B*, distributed on its surface can be obtained.

Contrasting CMPM to the novel reaction centrifugal mixed-powder method (RCMPM) proposed in the current study, the main difference is that, formation of the reinforcement particles in RCMPM occurs during the mold spinning by reaction. Namely, particles *B* and metal matrix *A* can be reacted as $mA + nB = A_mB_n$. Therefore, the temperature at which the powder/molten metal matrix react to form the reinforcements is the essential point in RCMPM.

Regarding the effect of FGMs-CM on the wear properties of the fabricated samples, Watanabe *et al.* [25] examined the wear properties of an Al-$Al_3Ti$ FGM manufactured by the CM. In particular, the influence of the oriented $Al_3Ti$ platelets in the matrix on the tribological behavior was analyzed. These Al-$Al_3Ti$ FGM presented anisotropic wear resistance when tested on different directions relative to the particles alignment as shown in Fig. 1.7 [25].

Suarez *et al.* [46] have reported the wear response of an Al-FGM reinforced with $AlB_2$ particles and produced by CM. The wear tests were conducted on the external and internal zones of the samples using ball-on disk test type. Results indicate that the hardness values and wear track analysis were consistent with the microstructural gradient. In effect, the higher volume density of reinforcing boride particles in the outer regions of the centrifugally cast samples translates into a higher hardness and higher overall wear resistance on those regions. On the other hand, the internal regions were fairly depleted of boride reinforcement particles and, thus, were subject to higher wear rates [44].

Sequeira *et al.* [29] have also fabricated Al-$Al_3Ti$ and Al-$Al_3Zr$ FGMs using the CSPM. It was found that the solid $Al_3Ti$ platelets in the melt were oriented with their platelet planes nearly normal to the centrifugal force direction. Using this fabrication method, both of the orientation and the compositional gradients can be altered to achieve the required properties.

Since the anisotropy of orientation of the reinforcement is likely to affect greatly the mechanical and physical properties of the composites, detailed knowledge of orientation distribution of the particles in FGMs is a requirement for predicting the mechanical properties of these materials [32]. Therefore, the current study will give a special attention to the relationship between the particles orientation and the mechanical properties of the Al-$Al_3Ti$ and Al-$Al_3Zr$ composites after processing by SPD and FGMs concepts.

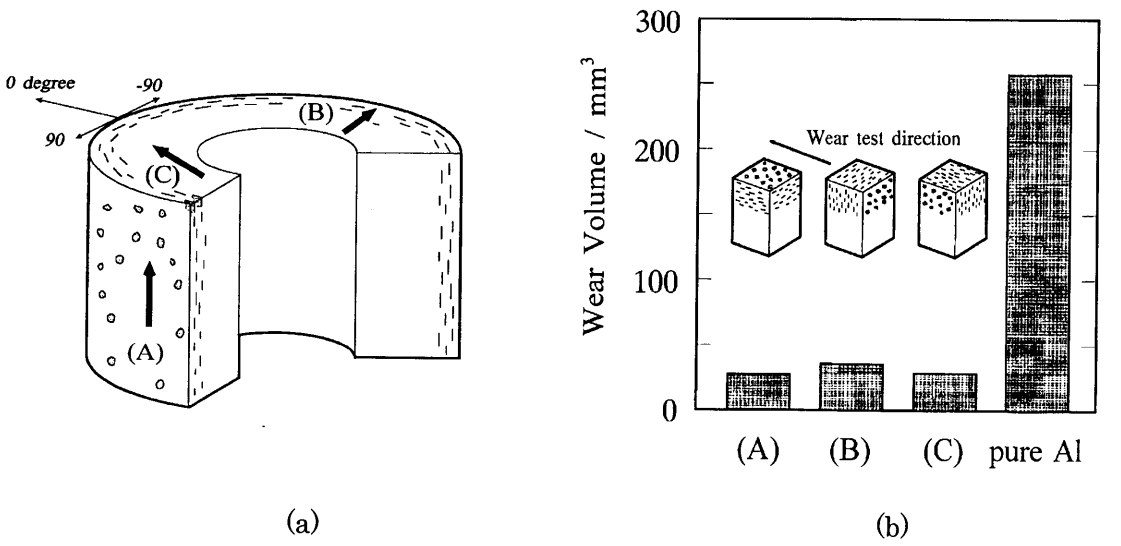


**Fig. 1.7. Schematic representation of a) the arrangement of $Al_3Ti$ particles and b) the wear test direction in an Al-$Al_3Ti$ FGM ring [25].**

## 1.3. Outline

In chapter- 2, the effect of processing Al-$Al_3Zr$ composite by ECAP on its anisotropic mechanical properties is investigated. As mechanical properties, hardness, wear resistance and compression strength properties were studied.

In chapter- 3, Al-$Al_3Ti$ composite was processed by ECAP using routes A and $B_C$ up to 8 passes of deformation. The influence of deformation by ECAP on the wear anisotropy of the composite is discussed.

In chapter-4, Al- $Al_3Zr$ FGMs were fabricated by CSPM under applied centrifugal force of $G$= 30, 60 and 120, where $G$ number is the centrifugal force magnitude. The wear anisotropy of the fabricated Al-$Al_3Zr$ FGMs and its relationship to the platelet particles orientation are explained.

In chapter-5, Al-5 mass% Ti FGMs were fabricated by the centrifugal solid-particle method under applied centrifugal force of $G$= 80. The wear induced plastic deformation of the

FGMs samples is investigated through studying the sub-worn surface morphology of the fabricated rings.

In chapter-6, effect of processing temperature on the microstructure and mechanical properties of Al-$Al_3Ti$ FGMs fabricated by CSPM and CISM are evaluated.

In chapter-7, Al-$Al_3Ti$ FGMs were fabricated by a novel RCMPM under different temperatures. Effect of RCMPM processing temperature on the formation of $Al_3Ti$ intermetallics, its morphology and its distribution in the fabricated Al-$Al_3Ti$ FGMs is examined.

In chapter-8, summary and general conclusions of the current research are presented.

## References:

[1] Widom M, Moriarty J. Physical Review B, 58 (1998) 14.

[2] Yamaguchi M, Inui H. $Al_3Ti$ and its L1 variations. In: Westbrook JH, Fleischer RL, editors. Structural applications of intermetallics compounds. New York: John Wiley, 1995. p. 151.

[3] Massalki T.B, Murry J.L, Bennet L.H, Baker H. Binary Alloy Phase Diagrams. Metals Park: ASM; 1986

[4] Das S.K. Al-Rich Intermetallics in Aluminum Alloys. In: Westbrook JH, Fleicher RL. Editors. Intermetallic Compounds, Vol 3, Structural Applications of. New York, Wiley; 2000. p. 175.

[5] Zedalis M, Fine M.E. Scripta Mater., 17 (1983) 1247.

[6] Villars P, Calvert L.D. Pearson's Handbook of Crystallographic Data fot Intermetallic Phases. Metals Park: ASM; 1985.

[7] Wang S.H, Kao P.W. Acta Mater., 46 (1998) 2675.

[8] Takeda M, Kikuchi T, Makihara S. J. Mater. Sci. Letters, 18 (1999) 631.

[9] Jinxu Z, Gengxiang H, Jiansheng W. J. Mater. Sci. Letters, 19 (2000) 1685.

[10] Moon K.I, Kim S.C, Lee K.S. Intermetallics, 10 (2002) 185.

[11] Karpets M.V, Milman Y.V, Barabash O.M, Korzhova N.P, Senkov O.N, Miracle D.B, Legkaya T.N, Voskoboynik I.V. Intermetallics, 11 (2003) 241.

[12] Langdon T.G. Rev. Adv. Mater. Sci.,13 (2006) 6.

[13] Valiev R.Z, Longdon T.G.Prog. Mater. Sci., 51 (2006) 881.

[14] Valiev R.Z, Estrin Y, Horita Z, Longdon T.G, Zehetbauer M.J, Zhu YT. JOM, 58 (2006) 33.

[15] Srinivasan R, Chaudhury P. K, Cherukuri B, Han Q, Swenson D, Gros P, Final Technical report, Oak Ridge National Laboratory, Oak Ridge TN.

[16] Segal V. M. USSR Patent No. 575892, (1977)

[17] Kim I-S. J. Mater. Proc. Tech., 113 (2001) 617.

[18] Beygelzimer Y, Varyukhin V, Orlov D, Efros B, Stolyarov V, Salimgareyev H, Ultrafine Grained Materials II; Edited by Y.T. Zhu, T.G. Langdon, R.S. Mishra, S.L. Semiatin, M.J. Saran, and T.C. Lowe. TMS, Warrendale PA, p. 43, (2002)

[19] Thomas W.M, Edward N.D, Needham J.C, Murch M.G, Smith P.T, Dawes, Christopher J, "Friction Stir Welding," GB Patent Application 9125978.8, Dec. 1991, US Patent 5460317, Oct. 1995

[20] Ghosh A. K, U.S.Patent- 4,721,537, January 26, (1988).

[21] Tsuji N, Saito Y, Utsunomiya H, Tanigawa S, Scripta Mater., 40 (1999) 795.

[22] Huang J. Y, Zhu Y. T, Jiang H, Lowe T. C. Acta Mater., 49 (2001) 1497.

[23] Wang S.H, Kao P.W. Scripta Mater., 40 (1999) 289.

[24] Watanabe Y, Yamanaka N, Fukui Y. Z. Metallkd., 88 (1997) 717.

[25] Watanabe Y, Yamanaka N, Fukui Y. Metall. Mater. Trans.A, 30A (1999) 3253.

[26] Watanabe Y, Fukui Y. Rec. Res. Devel. Metall. Mater. Sci., 4 (2000) 51.

[27] Watanabe Y, Fukui Y. Aluminum Trans., 2 (2000) 195.

[28] Watanabe Y, Eryu H, Matsuura K. Acta Mater., 49 (2001) 775.

[29] Sequeira P.D, Watanabe Y, Rocha L.A Mater. Sci. Forum, 492 (2005) 609.

[30] Sequeira P.D, Watanabe Y, Rocha L.A, Sol. Stat Phen. 105 (2005) 425.

[31] Watanabe Y, Kurahashi M, Kim I-S, Miyazaki S, Kumai S, Sato A, Tanaka S-i. Composites: Part A, 37 (2006) 2186.

[32] Pinto Z, MSc Thesis, University of Puert Rico Mayaguez Campus, 2006

[33] Hirai T., Processing of Ceramics, 17B, New York, NY, 1996, p. 293.

[34] Suresh S and Mortensen A. Fundamentals of Functionally Graded Materials- Processing and Thermomechanical Behavior of Graded Metals and Metal-Ceramic Composites. Cambridge: IOM Communications; 1998, p. 16

[35] Watanabe Y, Sato H, Fukui Y. J. Solid Mech. Mater. Eng., 2 (2008) 842.

[36] Watanabe Y, Sato R, Kim I.S., Miura S, Miura H. Mater. Trans., 46 (2005) 944.

[37] Langdon T.G, Furukawa M, Nemoto M, Horita Z. JOM, 52(2000) 30.

[38] Zhu Y.T, Langdon T.G. JOM, 56 ( 2004) 58.

[39] Fukui Y. JSME Inst. J. Series III, 34 (1991) 34.

[40] Fukui Y, Watanabe Y. Metal. Mater. Trans. A, 27A (1996) 4145.

[41] Watanabe Y, Yamanaka N, Fukui Y, Composites Part A, 29A (1998) 595.

[42] Yamagiwa K, Watanabe Y, Fukui Y, Kapranos P. Mater. Trans., 44 (2003) 2461.

[43] Watanabe Y, Sato R, Matsuda K, Fukui Y. Sci. Eng. Comp. Mater., 11 (2004) 185.

[44] Inaguma Y, Sato H, Watanabe Y. Mater. Sci. Forum, 631-632 (2010) 441.

[45] Sato H, Inaguma Y, Watanabe Y. Mater. Sci. Forum, 638-642 (2010) 2160.

[46] Suarez O.M, Melgarejo Z.H, Sridharan K. Composites Part A, 39A (2008) 1150.

# Chapter 2
# Anisotropic Mechanical Properties of Equal Channel Angular Pressed Al-$Al_3Zr$ Composite Containing Platelet Particles

## 2.1. Introduction

The application of severe plastic deformation (SPD) to metals and alloys provides a convenient procedure for achieving ultrafine grain sizes without introduction of any residual porosity [1-3]. As mentioned in Chapter 1, equal channel angular pressing (ECAP) is one of the developed SPD processing techniques [4-7]. By comparison with the conventional processing techniques, ECAP provides the capability of introducing large strains without changing the cross-sectional dimensions of the work-piece [8, 9]. Many metals and alloys have been deformed via ECAP and enhanced mechanical properties have been reported [10].

Based on the previous description of ECAP routes, section 1.2.1, in ECAP using route A the sample is not rotated between repetitive pressings while in route $B_C$ the sample is rotated by 90° between each press [11]. Therefore, homogenous structures can be obtained by route $B_C$ method and inhomogeneous structures will be generated by route A method. For example, Zhang *et al.* [12] has studied an ECAPed Al-5.7 mass% Ni eutectic alloy processed through route $B_C$ and route A methods. It was found that after ECAP processing by route $B_C$ method, the fine $Al_3Ni$ particles were homogeneously dispersed in Al matrix and the samples showed no clear anisotropic in tensile properties. After ECAP processing by route A method, however, the eutectic textures containing α-Al and $Al_3Ni$ fibrous dispersoids have highly anisotropic distribution and are proved to have significant anisotropy in tensile properties.

Some of the recent works [13] have focused on Al-$Al_3Ti$ composites including $Al_3Ti$ platelet particles and the effect of ECAP on the particles fragmentation has been investigated. It has been reported that, as the number of ECAP passes increases, the $Al_3Ti$ particles are fragmented and longitudinal direction of $Al_3Ti$ platelet particles is aligned towards the deformation direction. Generally, the mechanical properties of the alloys containing solid

particles are affected by its distribution. Therefore, if the platelet particles are heavily aligned to a direction, the mechanical properties of the alloy should have anisotropy.

In previous works of Watanabe *et al.* [14, 15], they have studied the anisotropy of the wear property in Al-$Al_3Ti$ functionally graded materials (FGMs) [16], containing $Al_3Ti$ oriented platelets. These FGMs were fabricated by centrifugal solid-particle method (CSPM). The Al-$Al_3Ti$ FGMs have graded distribution of the volume fraction and the orientation of $Al_3Ti$ platelet particles along centrifugal force direction inside the FGMs. It has found that Al-$Al_3Ti$ FGMs have anisotropic wear property due to the oriented distribution of the $Al_3Ti$ particles perpendicular to the centrifugal force direction. This means that the mechanical properties of the Al-$Al_3Ti$ FGMs have anisotropy because of the platelet $Al_3Ti$ particles which are aligned to a certain direction.

On the other hand, it has been reported [17] that Al-$Al_3Zr$ composite has similar structure to Al-$Al_3Ti$ composite. In this reported study, the fabricated Al-$Al_3Zr$ FGMs were characterized by the presence of $Al_3Zr$ platelet particles in Al matrix; those platelets were almost oriented to a direction normal to the centrifugal force direction. Therefore, if the Al-$Al_3Zr$ composite is severely deformed, the deformed alloy would have anisotropic mechanical property. Also, because the fragmentation of $Al_3Zr$ platelet particles would occur during the deformation process, the mechanical property of an Al-$Al_3Zr$ composite would be affected by its particle size.

Since particulate reinforced aluminum matrix composites are currently considered as promising tribological materials with applications in aerospace and automotive industries [18], it is of interest to study the mechanical properties of deformed Al-$Al_3Zr$ composites. Many studies were carried out on severely deformed Al-$Al_3X$ composites [10]. However, the mechanical properties of ECAPed Al-$Al_3Zr$ composites are still unclear.

In this chapter, the effect of processing Al-$Al_3Zr$ composites by ECAP on their anisotropic mechanical properties has been investigated. Al-$Al_3Zr$ composites processed by ECAP using routes A and $B_C$ were used for the investigation.

## 2.2. Experimental procedures

### 2.2.1. Preparation of ECAPed Al-$Al_3Zr$ samples

Rod shaped specimens with a diameter of 10 mm and a length of 60 mm were prepared from Al-5 mass% Zr alloy by casting at 900°C. Then the specimens were machined and homogenized at 550°C for 1 h followed by subsequent water quenching.

An ECAP die fabricated from tool steel with two cylindrical channels intersecting at 90° angle with an outer arc of curvature of 31.6° was used. The ECAP was conducted at room temperature with a pressing speed of 4mm/min and graphite oil was used as lubricant. The samples received an equivalent strain of about 1.0 for each pass through the die. ECAP were performed under routes A and $B_C$ for 4 and 8 passes.

The ECAPed samples were then cut along the deformation direction from its central position to obtain sections for microstructure and hardness investigations. Scanning electron microscope (SEM) was used to observe the distribution of $Al_3Zr$ particles in the ECAPed samples. Volume fraction of the $Al_3Zr$ particles was then measured by evaluating the area fraction of $Al_3Zr$ particles at random positions. The average length of $Al_3Zr$ particles was calculated using the linear intercept method. The aspect ratio of the particles was determined using image analysis software where; the aspect ratio is defined as the ratio of maximum and minimum lengths of the rectangle with smallest area that can be drawn around the particle.

### 2.2.2. Mechanical tests of ECAPed Al-$Al_3Zr$ samples

Using the ECAPed samples cut for microstructure investigation, Vickers hardness was measured at 5 N for 15 s at random positions. To study the anisotropy of the wear property of the ECAPed samples, the short samples were made for the wear test parallel to the deformation direction (WP direction in Fig. 2.1), while the long ones were made for the test perpendicular to the deformation direction (WN in Fig.2.1). The short and long samples have dimensions of 3.5mm x 3.5mm x 8mm and 3.5mm x 3.5mm x 20mm, respectively. Wear tests were carried out using block-on-disc type wear machine with a S45C and 170 Hv counter disc. The friction was done under reciprocal movement and the amplitude distance of 26 mm and frequency of 150

cycle/min were used. The applied load was 9.8 N and the total distance for the test was 468 m. The amount of wear was evaluated by calculating the samples weight loss due to wear.

The anisotropy in the compression strength of the ECAPed samples was also evaluated. Cubic samples of 3.5 mm x 3.5 mm x 3.5 mm were cut from the ECAPed samples. Two compression directions were chosen; parallel and perpendicular to the deformation axe of ECAP, named CP and CN respectively.

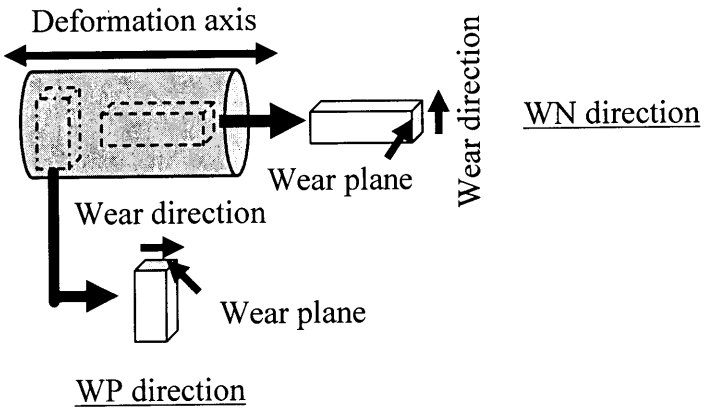


**Fig. 2.1. Wear test samples and directions**

## 2.3. Results and discussion

### 2.3.1. Microstructure of ECAPed Al-$Al_3Zr$ samples

Figure 2.2 is an SEM micrograph showing the original microstructure of Al-$Al_3Zr$ composites. The initial microstructure of Al-$Al_3Zr$ composite has coarse $Al_3Zr$ platelet particles randomly distributed in the Al matrix. Figures 2.3 (a) and (b) show the microstructure of the Al-$Al_3Zr$ composite ECAPed by routes A and $B_C$, respectively. After the as-cast Al-$Al_3Zr$ samples are deformed under the large strains of ECAP using routes A and $B_C$, $Al_3Zr$ platelet particles are severely fragmented and granular $Al_3Zr$ particles are observed. Figure 2.4 presents the average length of the $Al_3Zr$ particles as a function of the number of ECAP passes. The sizes

of $Al_3Zr$ particles in both of the specimens deformed with routes A and $B_C$ decrease with increasing the number of ECAP passes. This result is in agreement with Fig. 2.3.

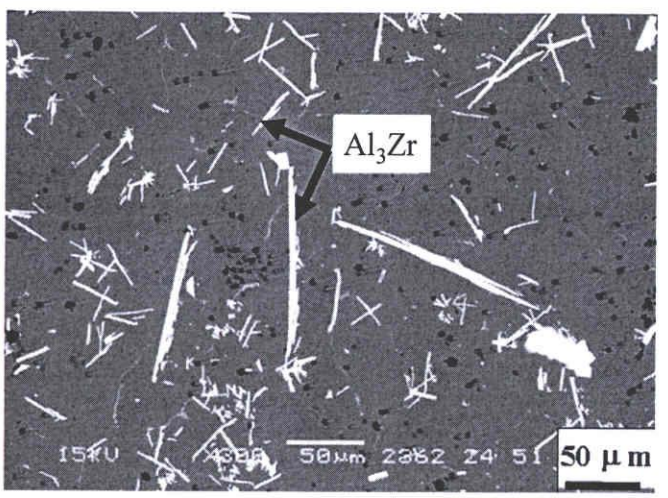


**Fig. 2.2. SEM image of the as cast Al-$Al_3Zr$ composite.**

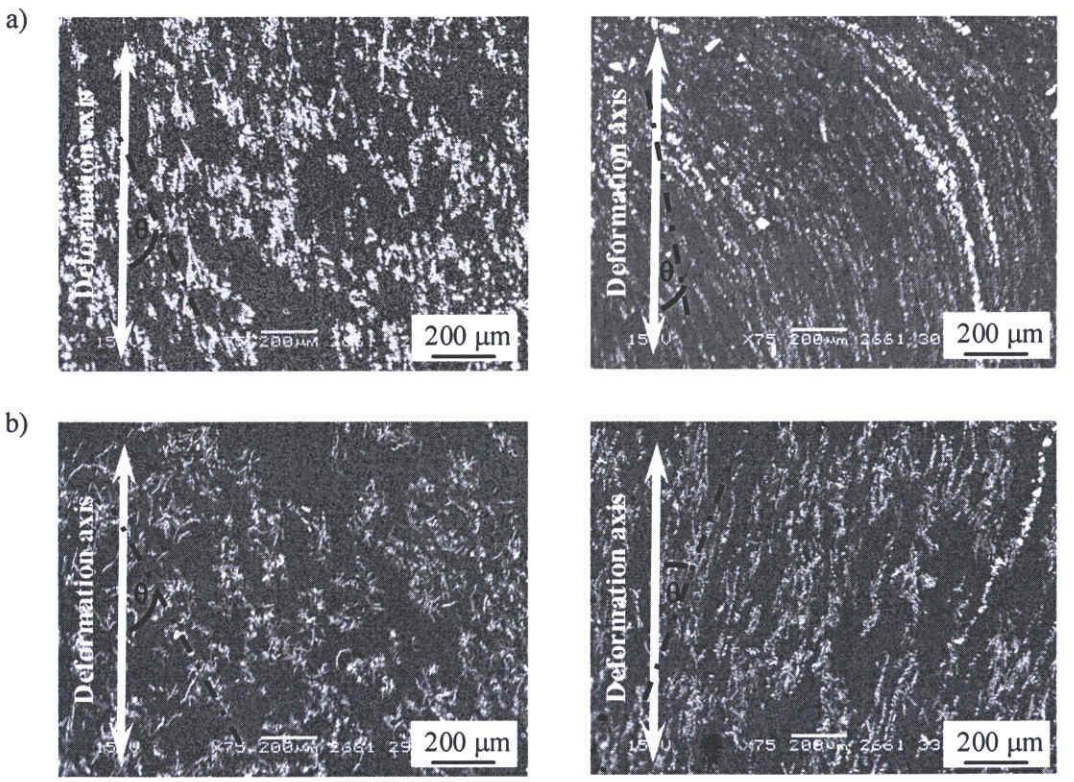


**Fig. 2.3. SEM micrographs of the ECAPed Al-5%Zr samples using a) route A and b) route $B_C$.**

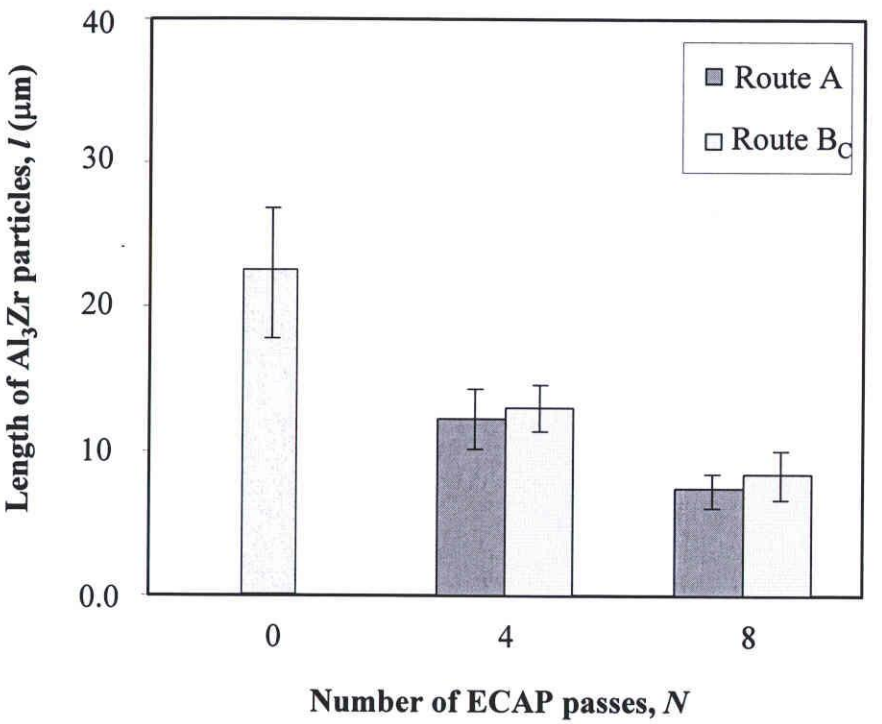


**Fig. 2.4. Mean size of $Al_3Zr$ particles versus number of ECAP passes.**

Figure 2.5 shows the variation of $Al_3Zr$ particles volume fraction in the ECAPed Al-$Al_3Zr$ specimens versus the number of ECAP passes. The volume fraction of the $Al_3Zr$ particles did not show much change with increasing the number of ECAP passes for both routes. However this volume fraction was slightly decreased at 8 passes of deformation. This is in accordance with the previous work for Zhang *et al.* [13], where the volume fraction of the $Al_3Ti$ particles in ECAPed Al-$Al_3Ti$ composite was decreased continuously with increasing the number of ECAP passes. This phenomenon has been explained through the severe fragmentation of the $Al_3Ti$ particles by ECAP, followed by the supersaturation of Ti into the Al matrix. This supersaturation was also confirmed for Al-$Al_3Zr$ FGMs as a result of severe wear test conditions as will be described in section 4.3.3. Considering this, further decrease of the $Al_3Zr$ volume fraction in the current samples is expected if larger strains were applied.

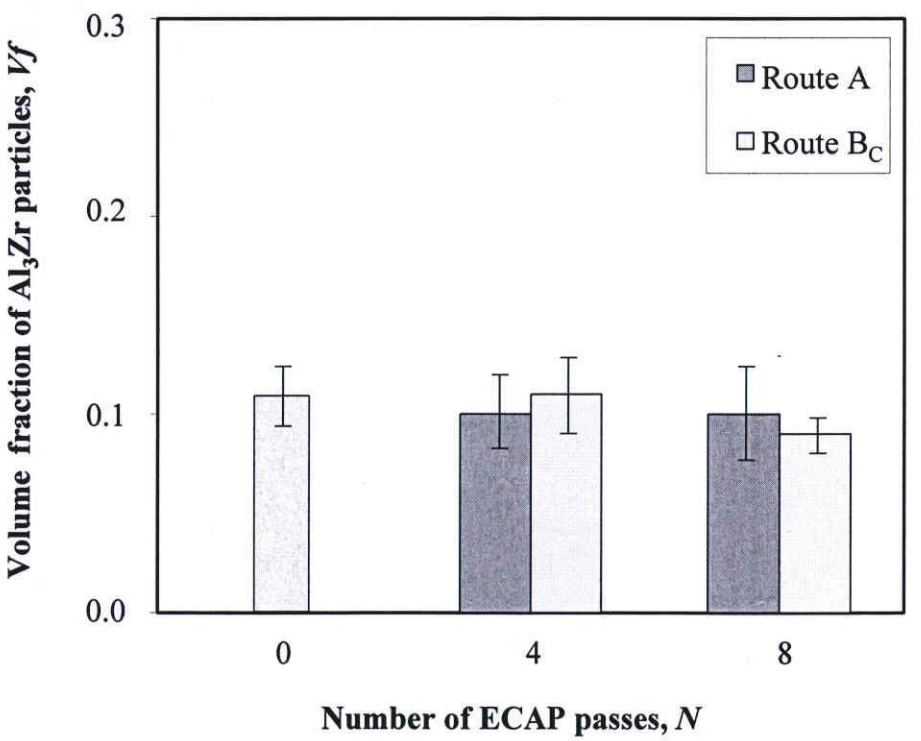


**Fig. 2.5. Volume fraction of the particles as a function in number of ECAP passes.**

Figure 2.6 presents the aspect ratio of $Al_3Zr$ particles in the samples before and after ECAP. Considering the aspect ratio shown in this figure along with the micrographs of Fig. 2.3, it can be remarked that the large strains induced by ECAP influence not only the particles size but also their shape relative to their original platelet shape. In case of the samples ECAPed using route A, shown in Fig. 2.3 (a), very fine granular particles arranged parallel to the deformation axe have been observed after 8 passes of deformation. Comparing to route A, the samples ECAPed by route $B_C$ showed higher aspect ratio at 4 passes thus some of $Al_3Zr$ particles retained its platelet shape after deformation. With further deformation, the samples prepared by the two routes attained the same aspect ratio at 8 passes of ECAP.

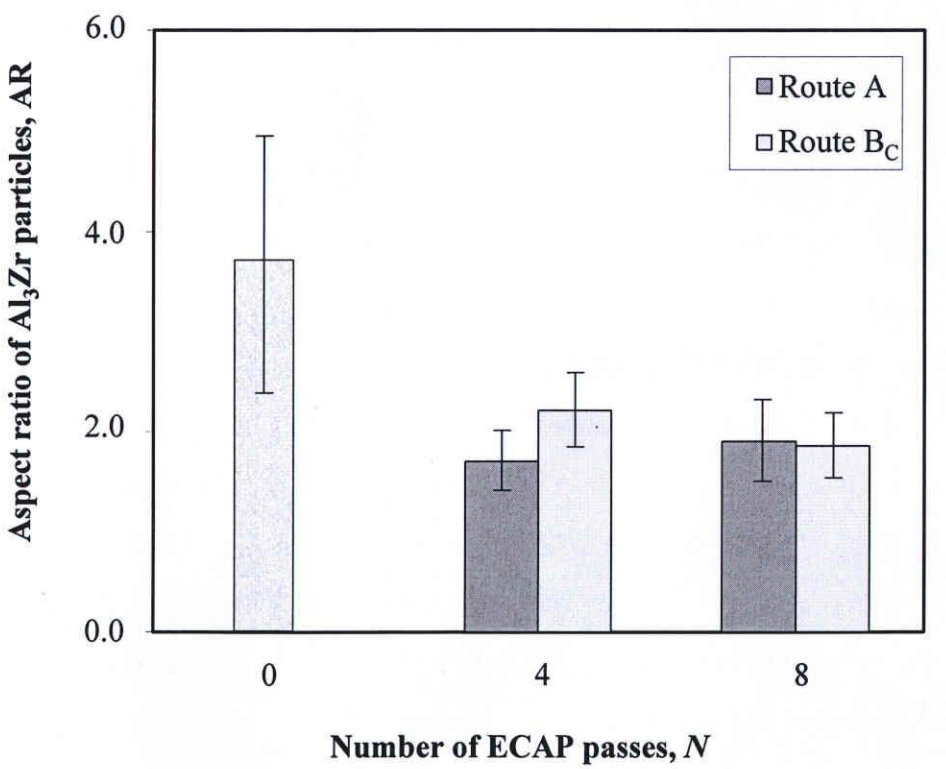


**Fig. 2.6. Average aspect ratio of $Al_3Zr$ particles versus number of ECAP passes.**

From Fig. 2.3 (a), a strong particles alignment parallel to the deformation axe can be observed in the samples ECAPed by route A. This is because of the unidirectional deformation of route A which accumulates a unidirectional shear strain in the specimens. On the other hand, the samples ECAPed by route $B_C$ showed smaller change in their alignment when the strain was doubled from 4 to 8, as shown in Fig. 2.3(b). This is attributed to the multi-directional strain reported for the samples deformed by route $B_C$ [10].

In order to study the alignment change of the $Al_3Zr$ particles during ECAP, the particles alignment was investigated by calculating the orientation parameter, $f_p$ for each Al-$Al_3Zr$ ECAPed sample. Considering the two-dimensional orientation and the angle $\theta$ between the deformation axis and the axis of an $Al_3Zr$ particle group as shown in the micrographs of Fig.3, the following equation was adopted for calculation of $f_p$ [16, 19, 20]

$$fp = [2\langle\cos^2\theta\rangle - 1], \quad \langle\cos^2\theta\rangle = \int_{-\pi/2}^{\pi/2} \cos^2\theta \; n(\theta) d\theta, \qquad (2\text{-}1)$$

where $n(\theta)$ is the orientation distribution function which specifies the fraction of the platelets within the element $d\theta$. The parameter $f_p$ becomes 0 for a random distribution, and it becomes 1 for the perfect alignment of the $Al_3Zr$ particles groups with their axis parallel to the deformation axis [16, 21]. The variation of $f_p$ as a function of number of ECAP passes is shown in Fig.2.7, different behavior of $f_p$ has been observed for the Al- $Al_3Zr$ samples ECAPed by routes A and $B_C$. In case of route A, the value of the orientation parameter has increased sharply from 4 to 8 passes. When the samples are deformed using route $B_C$, there was smaller difference with the increased number of passes. This is because ECAP using route $B_C$ is done by rotating the specimen 90° in the same direction, while route A is carried out without rotation. Therefore, the mechanical properties of ECAPed samples deformed by route A are expected to be anisotropic compared to those of route $B_C$.

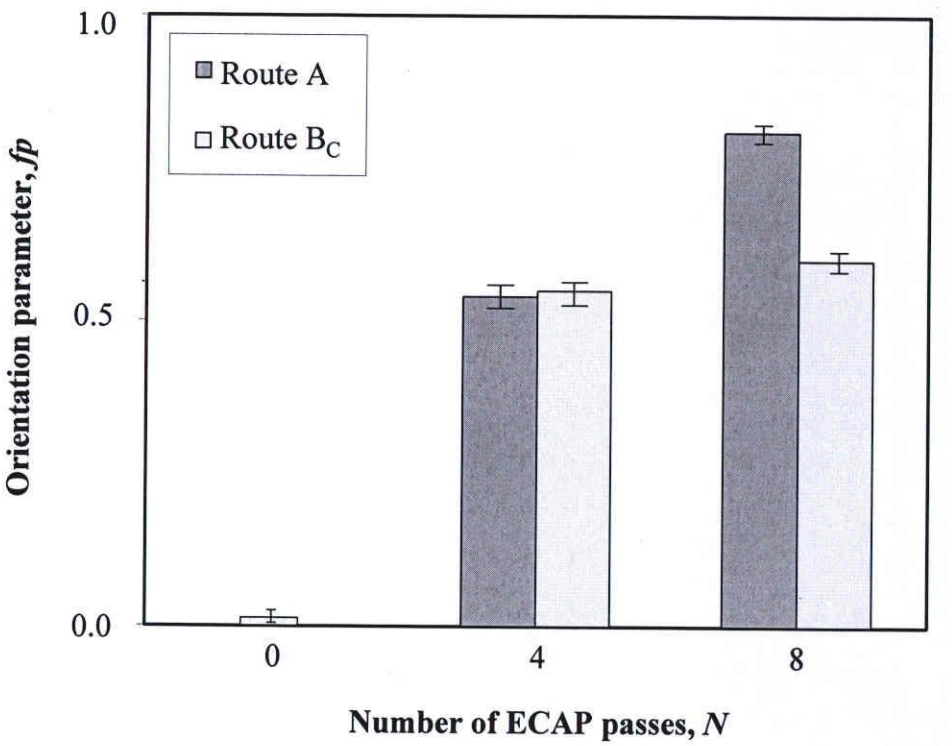


**Fig. 2.7. Calculated orientation parameter of the ECAPed Al-$Al_3Zr$ samples.**

### 2.3.2. Effect of ECAP on the hardness property

The hardness improvement of Al and its alloys deformed by ECAP were previously reported in several works [22-24]. According to their studies, ECAP enhances hardness of Al and Al alloys. This enhancement comes from the refinement of the matrix and the fragmentation of the secondary phases as a result of ECAP deformation.

Figure 2.8 shows variation of Vickers hardness (Hv) as a function of the number of ECAP passes. As can be seen in Fig. 2.8, a remarkable improvement of Hv by ECAP is observed. For the samples ECAPed by route A, Hv is increased with increasing the number of ECAP passes from 4 to 8 passes. On the other hand, small increment was observed with deformation by route $B_C$. This is because of the unidirectional strain of route A, which aligns the $Al_3Zr$ platelets parallel to the deformation axe and not distribute them in the matrix.

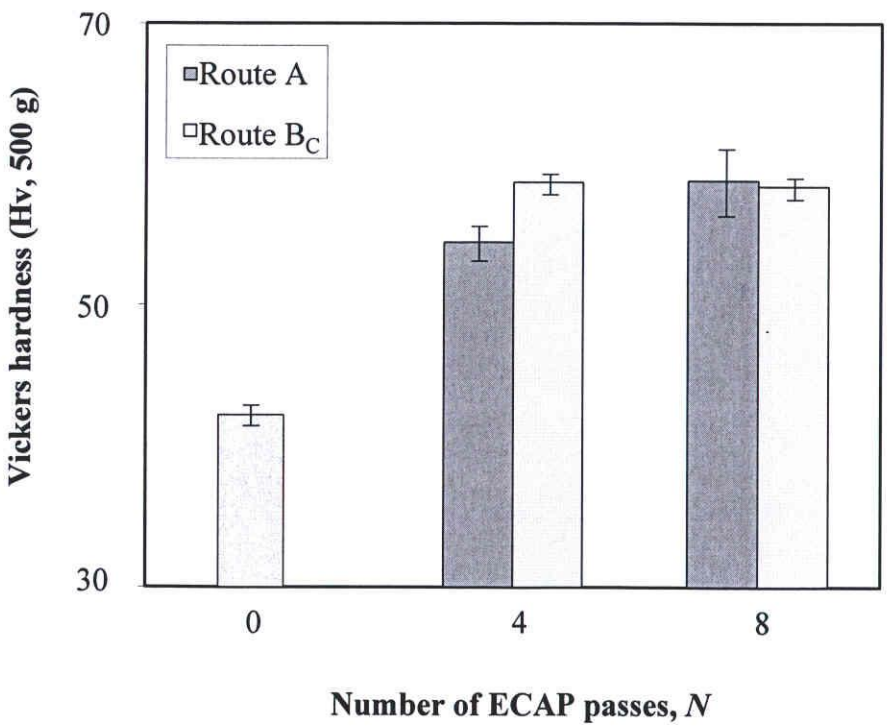


**Fig.2.8. Hardness, Hv of ECAPed Al-$Al_3Zr$ samples versus number of ECAP passes.**

### 2.3.3. Investigation of the anisotropic mechanical properties after ECAP

#### *2.3.3.1. Wear property*

Since the ECAP process influences the $Al_3Zr$ intermetallics size and their orientation relative to the deformation axe, it is expected that the anisotropy of wear property will be accordingly affected. In route A-ECAPed Al-$Al_3Zr$ samples, where a strong anisotropic microstructure and high value of orientation parameter could be observed, a large anisotropy in the wear property would be expected. However, the results of wear test for route A-ECAPed samples, in Fig. 2.9 (a), showed that the differences in the weight loss between WN and WP directions at 4 and 8 passes are negligible and the wear property of route A-ECAPed samples is almost isotropic. Watanabe *et al.* [15] have previously reported that the wear property of the metallic materials containing solid particles is strongly affected by the shape of particles. Based on it, if the $Al_3Zr$ particles in ECAPed samples deformed by route A were platelet in shape, the anisotropy of the wear property would be observed similar to the previous work for Watanabe *et al.* [14] on Al-$Al_3Ti$ FGMs.

Having seen the changes in the microstructure features of the ECAPed Al-$Al_3Zr$ samples after 8 passes A, in Fig. 2.10, it would be interesting to note the granular shape of the $Al_3Zr$ particles which resulted from their fragmentation during ECAP. Compared to the as-cast alloy, the aspect ratio of the $Al_3Zr$ particles in ECAPed samples was significantly decreased due to the large strains provided by ECAP. Considering the granular shape of $Al_3Zr$ particle while performing the wear test in different directions, small anisotropy in the wear property will be obtained.

Comparing the wear resistance of route A-ECAPed samples at 4 and 8 passes, Fig. 2.9 (a), it is observed that increasing the number of passes did not show much change in the weight loss of the ECAPed samples. Though, the significant increase of $f_p$ value from 4 to 8 passes using route A which resulted in a banded structure, as shown in Fig. 2.3(a), was expected to reduce the samples resistance to wear. However, the smaller size and the lower aspect ratio of the $Al_3Zr$ particles observed at 8 passes limited the negative effect of increasing $f_p$ on the wear resistance of the ECAPed samples. Therefore, the samples did not show much change between

4 and 8 passes of deformation.

Figure 2.9 (b) shows the weight loss of route $B_C$-ECAPed samples with increasing the number of ECAP passes. From this figure, small difference can be observed between the two testing directions WN and WP, and then the wear property has only small anisotropy for the samples processed by this route. This homogeneity of the deformed samples using route $B_C$ is attributed to the reported multi-directional strain of this route [5, 10].

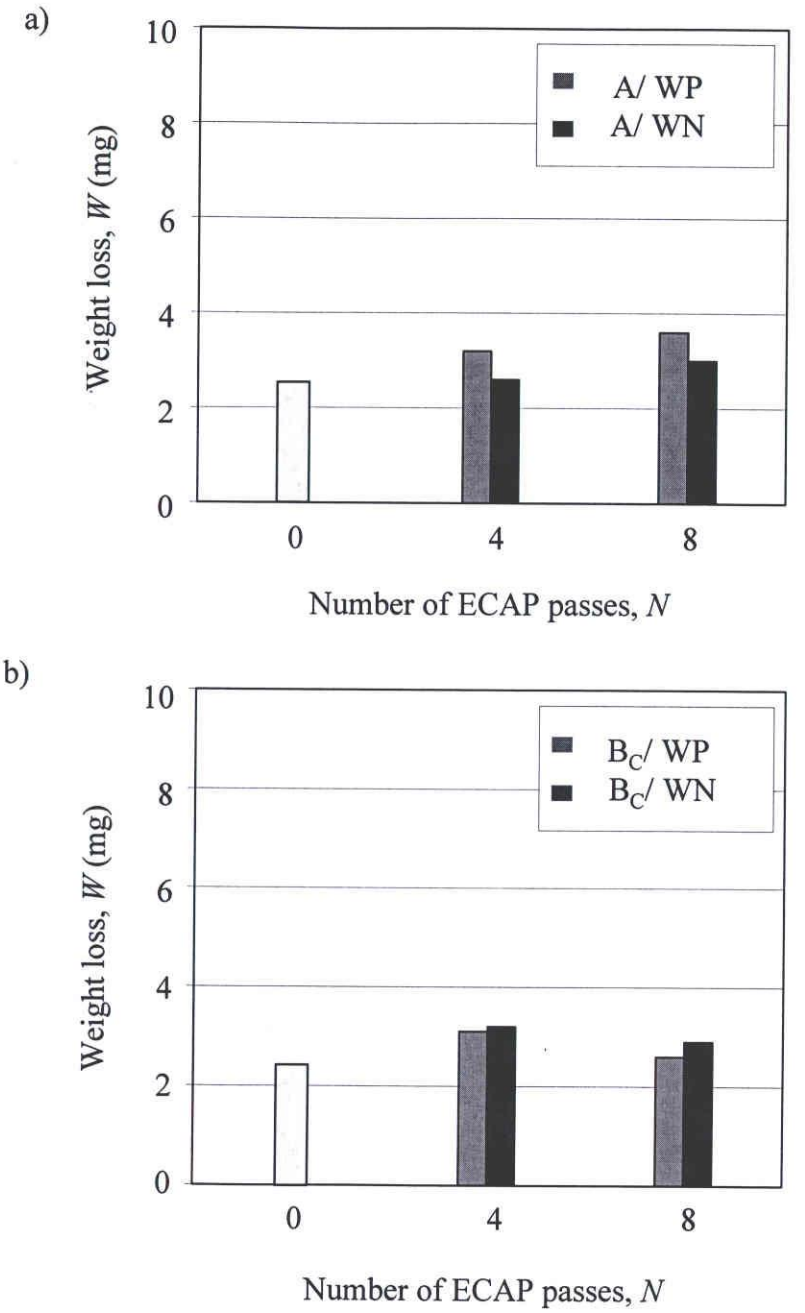


**Fig. 2.9. Variations of weight loss by wear of the specimens deformed with routes a) A and b) $B_C$, respectively.**

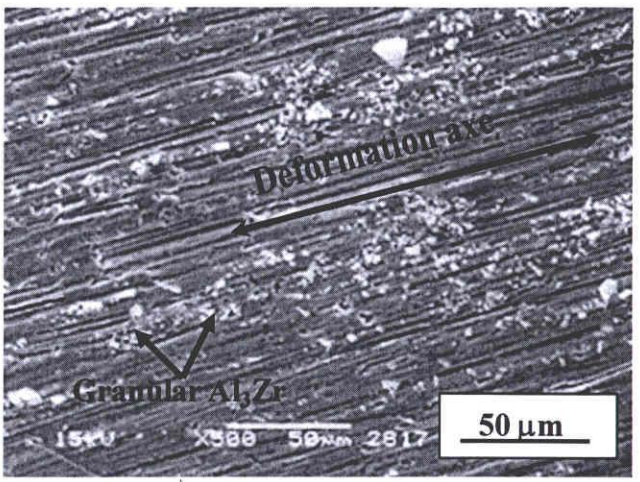


**Fig. 2.10. SEM micrograph of the ECAPed Al-5 mass% Zr samples after 8 passes A.**

### *2.3.3.2. Compression strength*

The anisotropy in compression strength of ECAPed Al-6061 and Al-7034 commercial Al based alloys were previously investigated by Xu *et al* [25] in X, Y and Z directions. This coordinate system was defined where X is the pressing direction, Y is perpendicular to both the flow direction and the side face of the billet and Z is normal to both the pressing direction and the top surface of the billet [25]. According to that study, it has been reported that the yield stresses of ECAPed Al-7034 alloy after 1 pass are similar for all compression directions, and that strain hardening rates of these specimen are slightly higher for the *Z* direction. On the other hand, after 6 passes of ECAP, both the yield stresses and the strain hardening rates are identical regardless of compression direction. In the present study, larger anisotropy would be expected due to the platelet shape of the $Al_3Zr$ particles. Stress strain curves obtained by compression test for some ECAPed Al-$Al_3Zr$ composite samples with routes A and $B_C$ are shown in Fig. 2.11. From this figure, it can be observed that the compression modulus for the Al/$Al_3Zr$ composite changes with changing the applied ECAP strain. It has been reported that the compression modulus can vary for the same material if this material has an anisotropic structure [26, 27]. Considering the investigated Al-$Al_3Zr$ composite; containing the platelet

$Al_3Zr$ particles whose orientation changes with increasing the applied strain, the compression modulus is expected to change accordingly.

Figure 2.12 shows that higher 0.2 % proof stresses are observed for the samples ECAPed by route A. This is because of the strong alignment of the granular $Al_3Zr$ particles group parallel to the deformation direction by route A. Comparing the results of route A samples shown in Fig. 2.12 for CP and CN testing directions, it is clear that compressing the samples parallel to the deformation direction achieved higher 0.2% proof stress than the normal testing direction. This observed anisotropy has decreased with increasing the applied strain from 4 to 8 passes although a stronger particles alignment was observed for the samples ECAPed with route A at higher strain. That is because the $Al_3Zr$ particles in the samples deformed at 8 passes under route A were severely fragmented and very fine granular particles were obtained as clear from Figs. 2.4 and 2.6. Therefore, effect of the particles shape on the anisotropy of the mechanical properties plays an important role in controlling the degree of anisotropy. Since the $Al_3Zr$ platelets became very fine granular particles, the difference between the two testing directions was decreased, and it is believed that this anisotropy can be diminished with further deformation.

In case of the samples deformed by route $B_C$, a little anisotropy can be remarked at 4 passes, then the difference in 0.2% proof stress between CP and CN directions became negligible at 8 passes of deformation. As a result, the multidirectional strain of route $B_C$ limited the anisotropy of the compression strength in the ECAPed Al-$Al_3Zr$ composites.

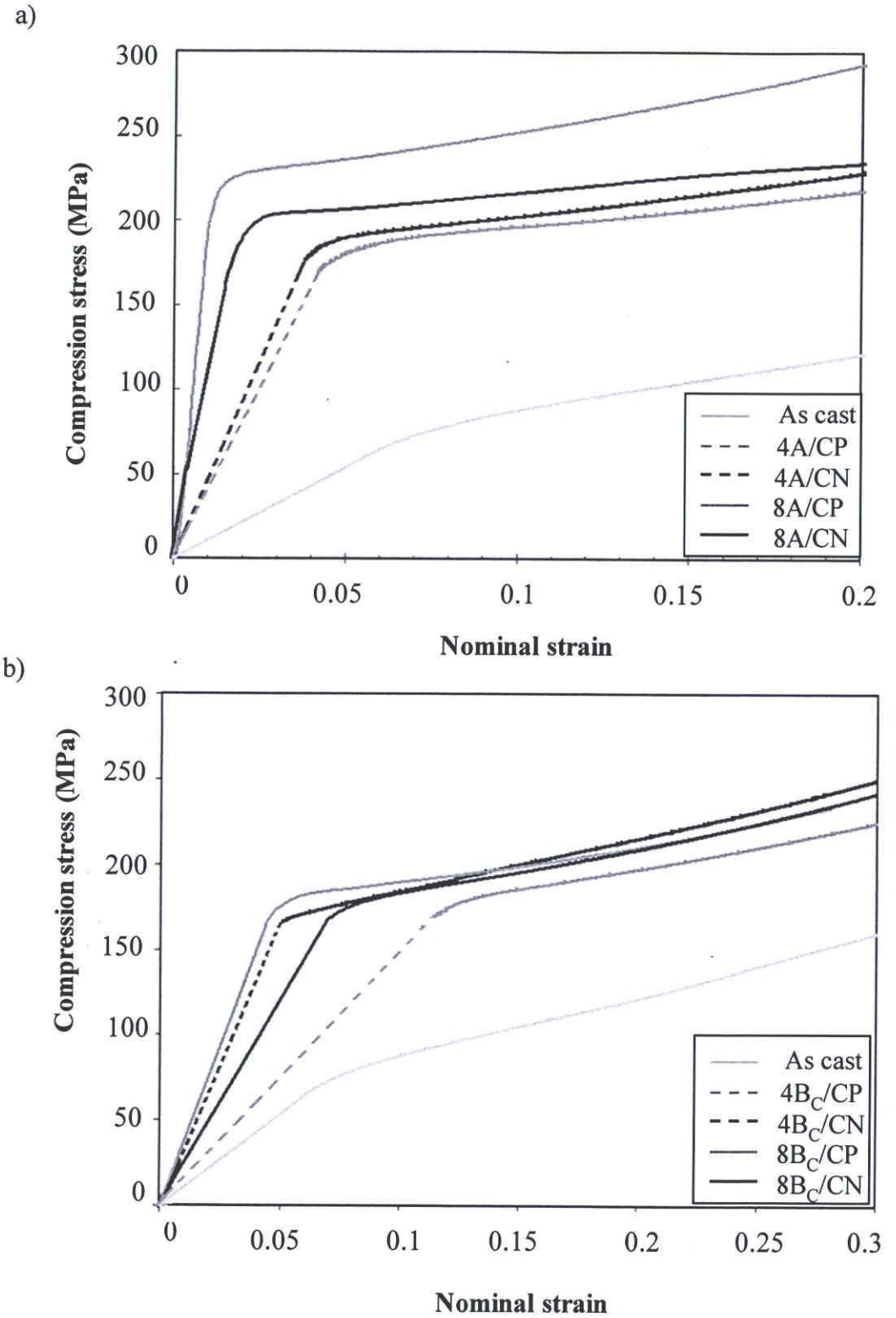


**Fig. 2.11. Compression stress-strain curves obtained from the compression of some ECAPed Al-$Al_3Zr$ samples using routes a) A and b) $B_C$.**

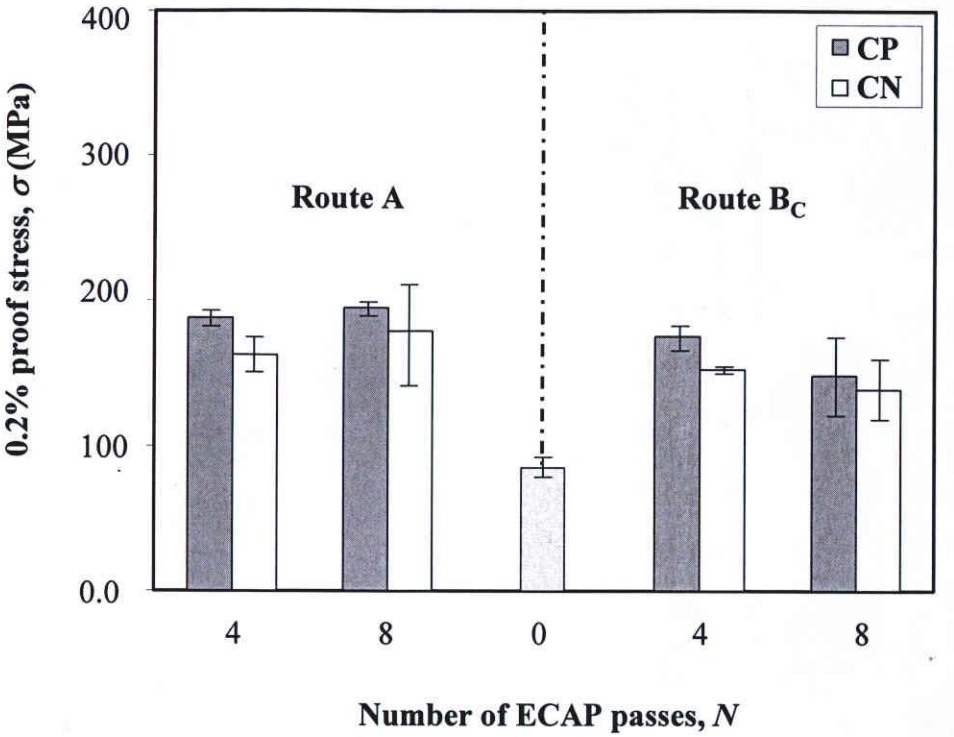


**Fig. 2.12. The 0.2% proof stress of the samples ECAPed by routes A and $B_C$ and compressed in the parallel and normal directions.**

## 2.4. Conclusions

Microstructural features of the ECAPed Al-$Al_3Zr$ composite have been studied and their effect on the anisotropy of the mechanical properties has been investigated. The results of this work can be summarized as follows;

(1) Microstructure of the ECAPed samples included severely fragmented $Al_3Zr$ particles. Shape of these platelets became granular with increasing the number of passes. The alignment of the particles parallel to the deformation axe was strongly dependent on the processing route.

(2) ECAPed samples by routes A and $B_C$ have small anisotropy in the wear property regardless of the processing route.

(3) Compression strength showed small anisotropy at 4 passes of ECAP using routes A and $B_C$. However, this anisotropy became negligible when the applied strain was doubled to 8 passes.

(4) The ECAP can play an essential role as a SPD process in controlling the anisotropy of the mechanical properties in the Al alloys containing platelet particles.

## References:

[1] Valiev R.Z, Islamgaliev R.K, Kuzmina N.F, Li Y, Langdon T.G. Scripta Mater., 40 (1999) 117.

[2] Furukawa M, Horita Z, Langdon T.G. Mat. Res. Soc. Symp., 634 (2001) B 8.5.1.

[3] Langdon T.G. Rev. Adv. Mater. Sci., 13 (2006) 6.

[4] Zhu Y.T, Lowe T.C. Mater. Sci. Eng., A291 (2000) 46.

[5] Raab G.J, Valiev R.Z, Lowe T.C, Zhu Y.T. Mater. Sci. Eng A, 382 (2004) 30.

[6] Valiev R.Z, Langdon T.G. Rev. Adv. Mater. Sci.,13 (2006) 15.

[7] Valiev R.Z, Estrin Y, Horita Z, Langdon T.G, Zehetbauer M.J, Zhu Y.T. JOM, 58 (2006) 33.

[8] Xu C, Langdon T.G. Scripta Mater., 48 (2003) 1.

[9] Kratochvíl J, Kružík M, Sedláček R, Sveshnikov A.M. Eng. Mech., 13 (2006) 261.

[10] Valiev R.Z, Langdon T.G. Prog. Mater. Sci., 51 (2006) 881.

[11] Nakashima K, Horita Z, Nemoto M, Langdon T.G. Acta Mater., 46 (1998) 1589.

[12] Zhang Z, Watanabe Y, Kim I-S. Mater. Sci. Tech., 21 (2005) 708.

[13] Zhang Z, Hosoda S, Kim I-S, Watanabe Y. Mater. Sci. Eng., A 425 (2006) 55.

[14] Watanabe Y, Yamanaka N, Fukui Y. Metall. Mater. Trans., 30A (1999) 3253.

[15] Watanabe Y, Sato H, Fukui Y. J. Solid Mech. Mater. Eng., 2 (2008) 842.

[16] Watanabe Y, Eryu H, Matsuura K. Acta Mater., 49 (2001) 775.

[17] Sequeira P.D, Watanabe Y, Rocha L.A. Mater. Sci. Forum, 492 (2005) 609.

[18] Wu J.M, Li Z.Z. Wear, 244 (2000) 147.

[19] McGee S.H., McCullough R. L. J. Appl. Phys., 55(1984) 1394.

[20] Watanabe Y. J. Comp. Mater., 36 (2002) 915.

[21] Watanabe Y, Yamanaka N, Fukui Y. Z. Metallkd, 88 (1997) 717.

[22] Valiev R.Z, Alexandrov I.V, Lowe T.C, Zhu Y.T. J. Mater. Res., 17 (2002) 5.

[23] Zhu Y.T, Langdon T.G. JOM, 56 (2004) 58.

[24] Horita Z, Ohashi K, Fujita T, Kaneko K, Longdon T.G. Adv. Mater. 17 (2005)1599.

[25] Xu C, Szaraz Z, Trojanova Z, Lukac P, Langdon T.G. Mater. Sci. Eng. A, 497 (2008) 206.

[26] Nayfeh A.H, Fiber Sci. and Tech., 10 (1977) 195.

[27] Davis J.R.(Eds.), Tensile testing, 2nd Edition, ASM International, Materials park, Ohio, 2004, p. 95.

# Chapter 3
# Investigation of Wear Anisotropy in Equal Channel Angular Pressed Al-$Al_3Ti$ Composite

## 3.1. Introduction

Severe plastic deformation (SPD) of metals and alloys has been reported to refine their structures by the intensive plastic strain imposed on the samples [1]. Moreover, some researches revealed the influence of SPD intensive strain on the microstructure orientation in some metallic alloys [2, 3]. This oriented microstructure may result in anisotropic mechanical properties in the deformed samples as explained in the previous chapter. Therefore, if a severely deformed Al-$Al_3Ti$ composite was selected for tribological applications, the anisotropy of its wear property should be carefully investigated.

The microstructure and texture evolution of an Al-$Al_3Ti$ composite equal channel angular pressed (ECAPed) with routes A and $B_C$ have been investigated by Watanabe *et al.* [4]. According to their study, microstructure of ECAPed samples by route A has highly anisotropic distribution of $Al_3Ti$ particles while route $B_C$ samples have homogeneous distribution of $Al_3Ti$ particles.

Considering the wear property of the ECAPed Al-$Al_3Ti$ composite based on the distribution of $Al_3Ti$ particles, it is expected that route A-ECAPed Al-$Al_3Ti$ composite will have anisotropy in its wear property. This is because the mechanical properties of the particle reinforced composite depend on the distribution and orientation of the reinforced particles [5, 6].

In this study, Al-5 mass% Ti composite was processed by ECAP with routes A and $B_C$ up to 8 passes. Using the ECAPed Al-$Al_3Ti$ composites deformed with different routes, the anisotropy in the wear property of ECAPed Al-$Al_3Ti$ composites was investigated. In spite of the alignment of $Al_3Ti$ platelet particles to the shearing direction during ECAP, a small anisotropy in the wear property of the deformed Al-$Al_3Ti$ composites has been observed.

## 3.2. Experimental procedure

### 3.2.1. Preparation of ECAPed Al-$Al_3Ti$ samples

Prior to processing by ECAP, rod-shaped ECAP specimens of Al-5 mass% Ti alloy with a diameter of 10 mm and a length of 60 mm were prepared by casting at 750°C and machining. The specimens were homogenized at 550°C for 1h and subsequently air-cooled. An ECAP die fabricated from tool steel with two circular cross-sections channels intersecting at 90° angle and a 36° outer arc of curvature was used [7] as shown in Fig. 3.1. The ECAP was conducted with a pressing speed of 4mm/min at room temperature using graphite as lubricant. An equivalent strain of about 1.0 was introduced into the sample for each pass through die [8]. Using the rod-shaped Al-$Al_3Ti$ composites, ECAP was carried out up to 8 passes by route A and route $B_C$.

### 3.2.2. Microstructural evaluation of specimens after ECAP

The ECAPed samples were cut along the pressing axis from its central position to obtain sections for microstructure and hardness investigations. Scanning electron microscope (SEM) was used to observe the distribution of $Al_3Ti$ particles in the ECAPed samples at random positions. The volume fraction of the $Al_3Ti$ particles was then measured by evaluating the area fraction of $Al_3Ti$ particles. The average length of $Al_3Ti$ particles was calculated using the linear intercept method. The particles aspect ratio was determined using image analysis software (Azo-Kun). The aspect ratio is defined as the ratio of maximum and minimum lengths of the rectangle with smallest area that can be drawn around the particle. The angle between the fragmented $Al_3Ti$ particles group and the deformation direction was measured at random positions in order to study the effect of ECAP on the particles alignment. X-ray diffraction analysis was used to investigate the effect of increasing ECAP strain on the $Al_3Ti$ peak in the ECAPed Al-$Al_3Ti$ samples.

### 3.2.3. Wear tests of ECAPed Al-$Al_3Ti$ samples

To study the anisotropy of the wear property of the ECAPed samples, two kinds of

specimens were cut at different directions relative to the deformation axis. The short specimen has a wear plane parallel to the deformation axis while the long one was cut normal to this axis. The short and long samples have dimensions of 3.5 mm x 3.5 mm x 8 mm and 3.5 mm x 3.5mm x 20 mm, respectively. The wear tests were carried out in X and Y directions, named PP and NN, respectively, as also shown in Fig. 3.1. The wear tests were performed using block-on-disc type wear test. The counter part was an S45C disc with 170 Hv hardness and the test was made under reciprocal line movement. Amplitude distance of the reciprocal movement was 26 mm and its frequency was 150 cycle/min. The load and total distance for the wear tests was 9.8 N and 468 m, respectively. The amount of wear was evaluated by weighing the samples before and after wear test.

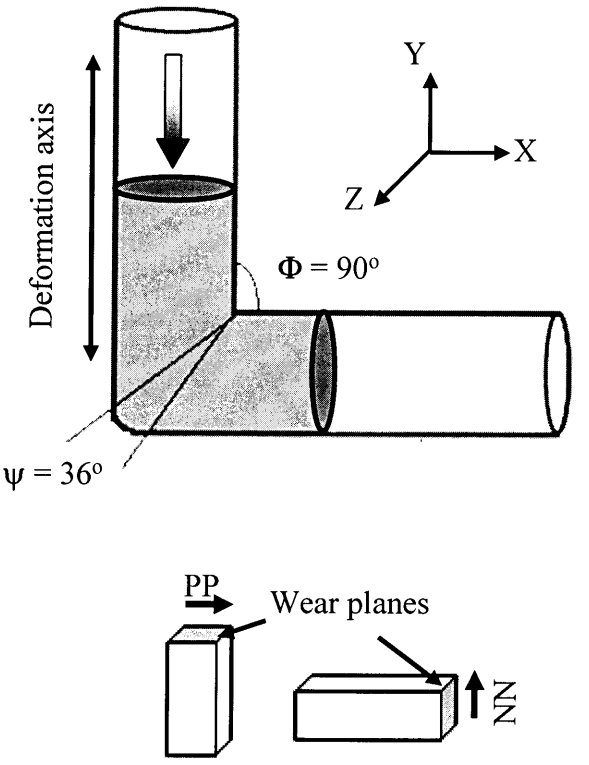


**Fig. 3.1. Schematic illustration of ECAP showing the wear test samples and the wear directions; PP and NN.**

## 3.3. Results and discussion

### 3.3.1. Microstructure of ECAPed Al-$Al_3Ti$ specimens

Figure 3.2(a) is an SEM micrograph showing the original microstructure of Al-$Al_3Ti$ composite where coarse $Al_3Ti$ platelet particles [9] were observed randomly distributed in the Al matrix. Figures 3.2 (b) and (c) show the microstructure of Al-$Al_3Ti$ composite ECAPed by routes A and $B_C$ respectively at 4 and 8 passes of deformation observed on the plane parallel to the pressing axis. After the as-cast Al-$Al_3Ti$ composite samples have been deformed under the large strains of ECAP, the $Al_3Ti$ platelet particles were severely fragmented and granular $Al_3Ti$ particles have been observed.

Figures 3.3 (a) and (b) shows the average size of $Al_3Ti$ particles and their aspect ratio as a function in the number of ECAP passes. It is remarked that the size of $Al_3Ti$ particles in both of the specimens deformed with routes A and $B_C$ decreased with increasing the number of ECAP passes as shown in Fig. 3.3(a). In addition, the aspect ratio of $Al_3Ti$ particles steeply decreased when deformed using both of ECAP routes (see Fig. 3.3(b)). Moreover, the common shape of the $Al_3Ti$ particle is changed from platelet to granular shape as can be observed from the magnified micrograph of route A sample after 4 passes of deformation, as shown in Fig. 3.4.

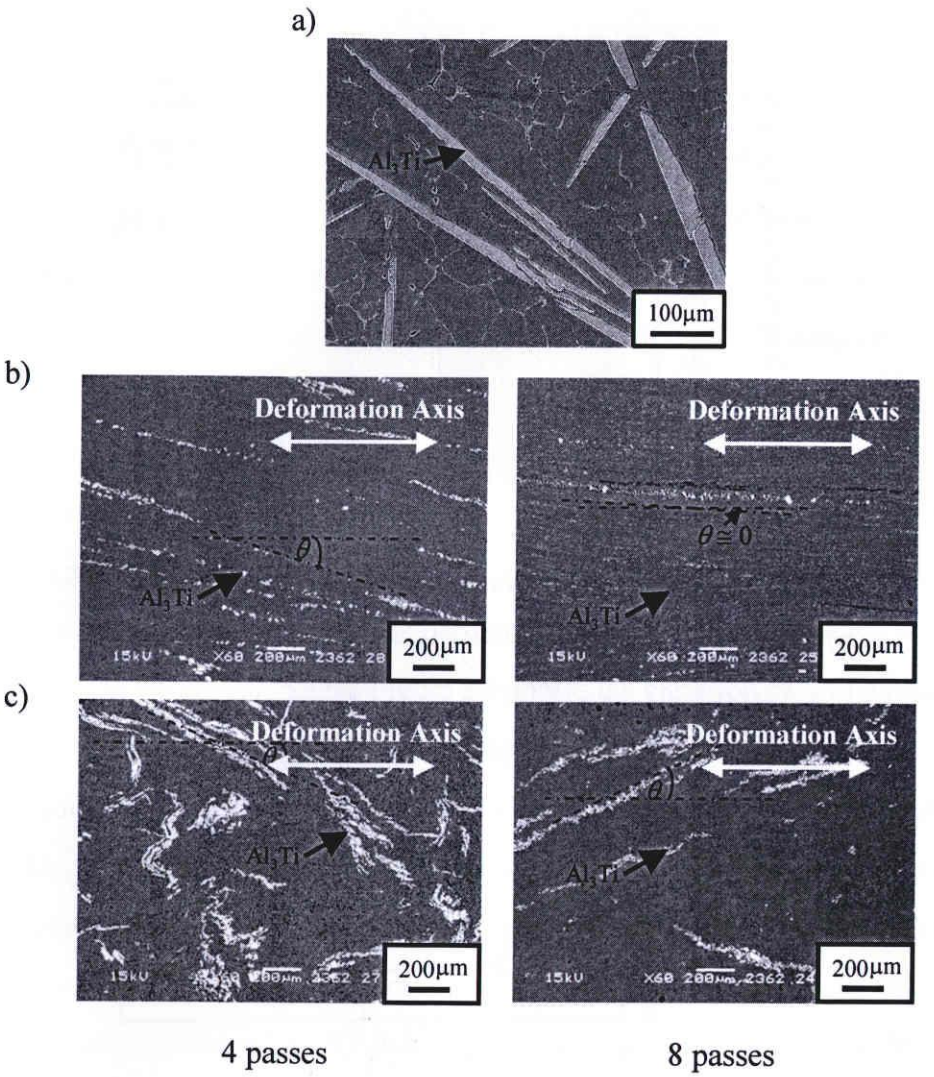


**Fig. 3.2. SEM photographs showing microstructure of a) As cast Al-$Al_3Ti$ composite, b) Route A and c) Route Bc ECAPed samples.**

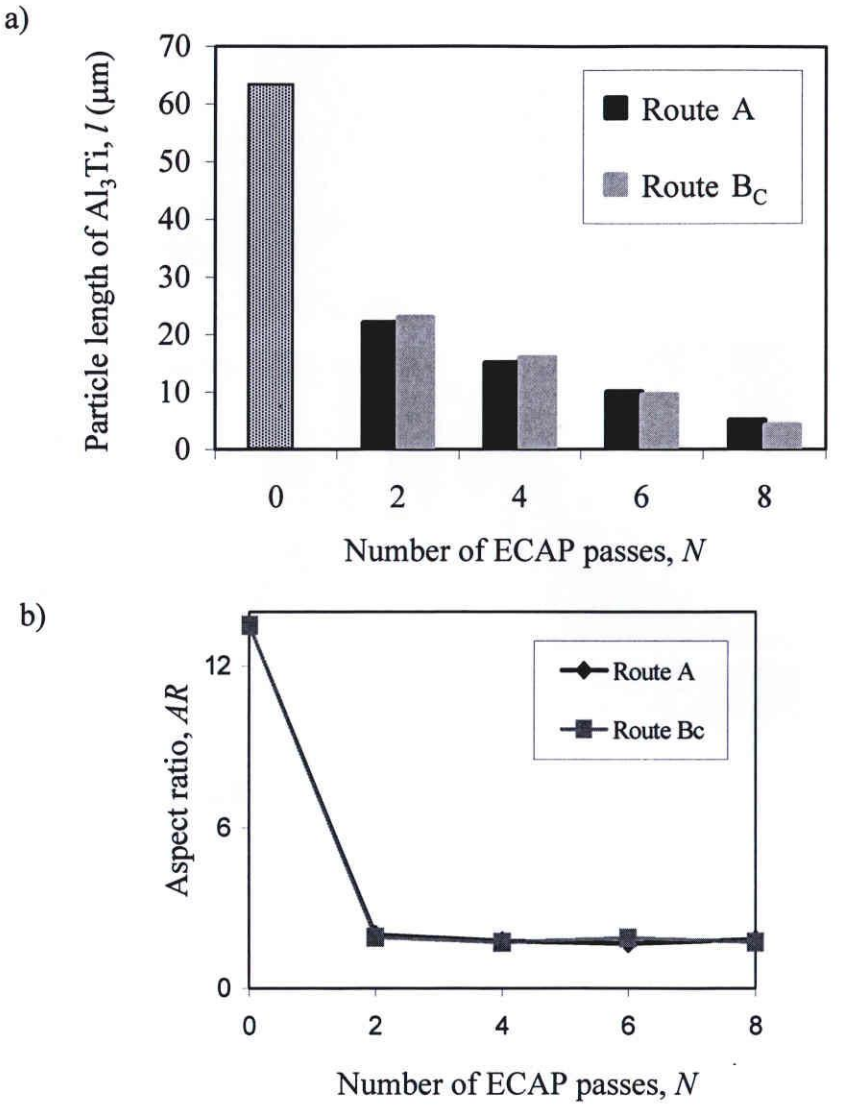


**Fig.3.3. Quantitative measurements of a) Mean size and b) Aspect ratio of $Al_3Ti$ particles versus number of ECAP passes on the plane parallel to the pressing axis.**

Comparing the microstructure of routes A and $B_C$ samples at 8 passes of deformation, micrographs of route A (Fig. 3.2 (b)) showed fine granular $Al_3Ti$ particles strongly aligned along the deformation axis and the initial shape of these $Al_3Ti$ particles was not observed anymore. On the other hand, in ECAPed specimen with route $B_C$, the alignment of the $Al_3Ti$ particles didn't show a significant change when the strain increased from 4 to 8. This difference of microstructure comes from the type of strain induced by ECAP. Route $B_C$ accumulates a multi-directional shear strain in the samples, while route A deform it through a unidirectional strain [10]. Therefore, the ECAPed microstructure will be different. In order to investigate the alignment change of $Al_3Ti$ particles during ECAP, a Herman's orientation parameter, $f_p$ [11, 12] was calculated from eq. (2.1), section; 2.3.1. The angle between the deformation axis and the axis of an $Al_3Ti$ particle group, $\theta$, is shown in Fig. 3.2. As previously defined, $f_p$ becomes 0 for a random distribution, and it becomes 1 for perfect alignments with the axis of $Al_3Ti$ particle groups parallel to the deformation axis. Figure 3.5 shows the variation of $f_p$ as a function of the number of ECAP passes evaluated on the plane parallel to the deformation axis.

It is clear that the behavior of $f_p$ for ECAPed Al-$Al_3Ti$ samples is different between routes A and $B_C$. In both of the ECAPed specimens at 2 passes, $f_p$ was around 0.4 and then this value continuously increased with further deformation by route A and the alignment of $Al_3Ti$ particles becomes almost parallel to deformation axis at 8 passes of ECAP. In case of route $B_C$, $f_p$ at 2 and 6 passes showed relatively larger $f_p$, while at 4 and 8 passes smaller $f_p$ has been observed. However, a relatively constant trend can be considered for the overall $f_p$ values from 2 to 8 passes of ECAP. This result is in accordance with the reported homogeneity of route $B_C$ samples and that anisotropic structure of route A specimens [8, 13].

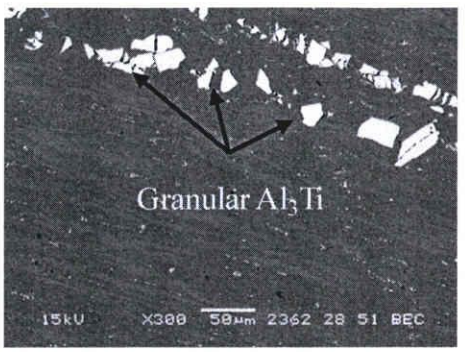


**Fig. 3.4. SEM micrograph of ECAPed Al-$Al_3Ti$ samples after 4 passes of route A.**

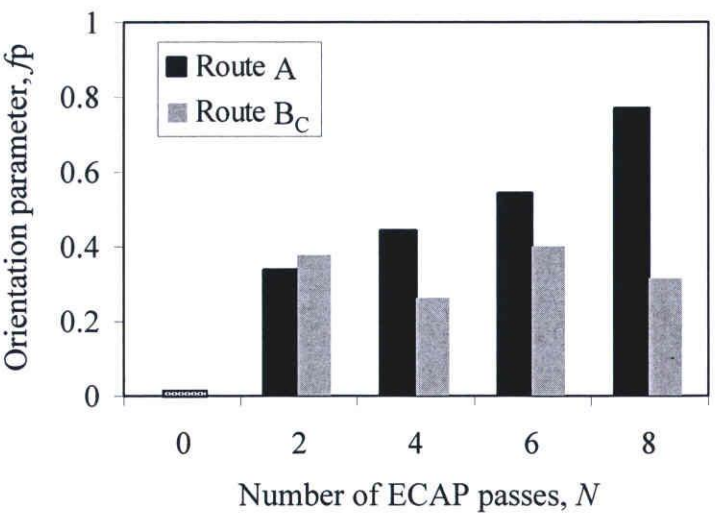


**Fig. 3.5. The change in the calculated orientation parameter of the ECAPed Al-$Al_3Ti$ samples with increasing number of ECAP passes.**

In a study by Zhang *et al.* [1] on ECAPed Al-Ti alloy specimens, they have observed that the volume fraction of $Al_3Ti$ particles decreased with increasing ECAP strain up to 15 using route $B_C$. Moreover, Watanabe *et al.* [14] and Sato *et al.* [15] have observed the same phenomenon for worn Al-Ti alloy specimens. They have concluded that the decrease in the $Al_3Ti$ particles volume fraction is caused by the severe fragmentation of $Al_3Ti$ particles due to large strains of ECAP followed by the supersaturation of Ti into the Al matrix. Valiev *et al.* [16] also reported that it is reasonable to expect evidence for the formation of metastable states during ECAP associated with the generation of supersaturated solid solutions, disordering or even amorphisation due to the large strain intensity.

In the current investigation, minor decrease was also observed in the $Al_3Ti$ particles volume fraction of route $B_C$ samples (from ~ 0.11 at 0 pass to ~ 0.096 at 8 passes $B_C$) which may be occurred by the same mechanism. However, this phenomenon could not be found in the samples ECAPed using route A. In order to confirm this result, XRD diffraction patterns of the ECAPed samples were obtained and presented in Fig. 3.6. The results show that the obvious peaks of Al and $Al_3Ti$ phases exist in the sample before ECAP. The $Al_3Ti$ peaks around 21°, 25°, 39° and 47° are obviously weakened with increasing the number of ECAP passes using route $B_C$. These weakened peaks explain the small decrease in the $Al_3Ti$ particles volume fraction when the samples were severely sheared by route $B_C$.

On the other hand, the same $Al_3Ti$ peaks became even stronger when route A of ECAP was used. This difference between route A and route $B_C$ also comes from the difference in the strain accumulated in the sample using the two ECAP routes. In case of route A, there is a cumulative building-up of unidirectional shear strain in each separate pass through the die. On the contrary, route $B_C$ is a redundant strain process where a multi directional shear strain is restored in the sample every 3 passes [16]. This in its turn alters the direction in which $Al_3Ti$ particles can be easily broken and dissolve Ti into the Al matrix.

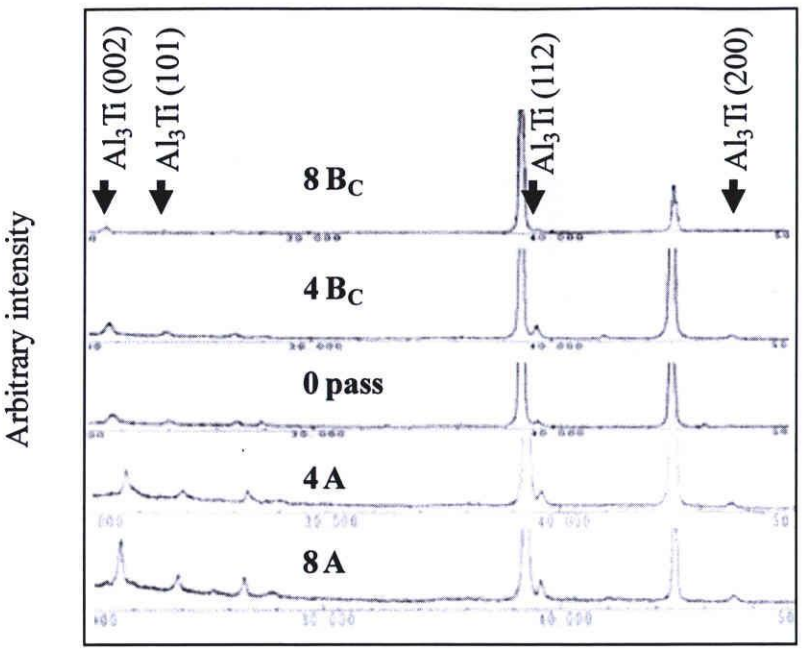


**Fig. 3.6. XRD patterns of the ECAPed Al-$Al_3Ti$ samples.**

### 3.3.2. Wear anisotropy of ECAPed Al-$Al_3Ti$ composites

The variations in weight loss by wear of routes A and Bc ECAPed samples using block-on-disc wear test are shown in Fig. 3.7 and Fig. 3.8, respectively. In the non-deformed samples, the presence of the very large intermetallics particles act as load-supporting elements preventing the soft matrix to become directly involved in the wear process, similar to particulate reinforced composites [17]. Upon further deformation, with a continued reduction in the size of $Al_3Ti$ particles and their alignment in bands along the deformation direction, a decrease in the wear resistance is observed in PP direction. This is due to the loss of load bearing capabilities of the particles which caused an increased wear rate accordingly. However, with increasing the applied strain up to 6, the particles will be further refined and show its strengthening effect on the matrix reducing the weight loss in the direction parallel to the

deformation direction [18, 19]. This was not the case for the NN direction where the wear rate increased at 2 passes of deformation then remained almost constant with increasing the applied strain. This can be attributed to the observed banded microstructure shown in Figs. 3.3 (b) and (c), which in its turn makes the contact between the sample block and the disc, occurs in successive bands of reinforced and non reinforced regions.

Comparing the weight loss for the two test directions shown in Fig. 3.7 and Fig. 3.8, it is observed that the wear property in the deformation direction, PP is consistently better than that for NN direction for both of routes A and $B_C$ samples. However, these differences in the wear property between NN and PP directions are considered negligible. Therefore, it can be said that the ECAPed samples do not have large anisotropic wear property regardless of the processing route.

The anisotropy in the wear property has been reported for Al-$Al_3Ti$ functionally graded materials (FGMs) with aligned $Al_3Ti$ particles [14]. In that study, the anisotropic wear property of the FGMs was dependent on the applied wear direction relative to $Al_3Ti$ particles. This is because $Al_3Ti$ particles were groups of coarse platelet particles aligned normal to the centrifugal force direction and distributed gradually in the fabricated FGMs. The schematic illustration of Al-$Al_3Ti$ FGM sample is shown in Fig. 3.9 (a), where the coarse aligned $Al_3Ti$ platelet particles can be observed on planes (OP1 and OP2) of the sample. In the current ECAPed Al-$Al_3Ti$ composites, $Al_3Ti$ particles group has also been aligned in a direction close to the deformation direction. However, the fragmentation of $Al_3Ti$ platelet particles by the large strain of ECAP has refined their size and changed their shape to the granular morphology, as obvious on planes (OP1 and OP2) shown in Fig. 3.9(b). Comparing the reported microstructure of Al-$Al_3Ti$ FGMs [14] with the current ECAPed Al-$Al_3Ti$ composite, only small anisotropy can be, therefore, expected in the wear property of ECAPed Al-$Al_3Ti$ samples when tested on PP and NN directions.

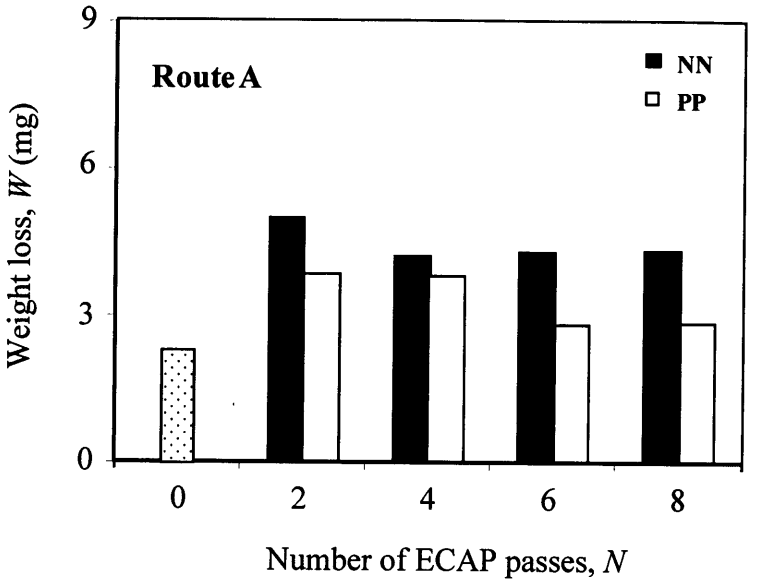


**Fig. 3.7. Weight loss during block-on-disc wear test of route A ECAPed Al-$Al_3Ti$ alloy samples.**

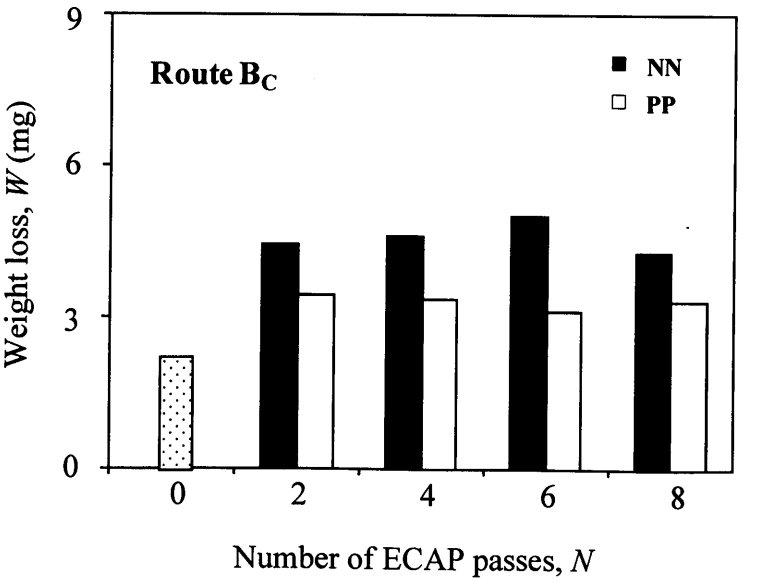


**Fig. 3.8. Weight loss during block-on-disc wear test of route $B_C$ ECAPed Al-$Al_3Ti$ alloy samples.**

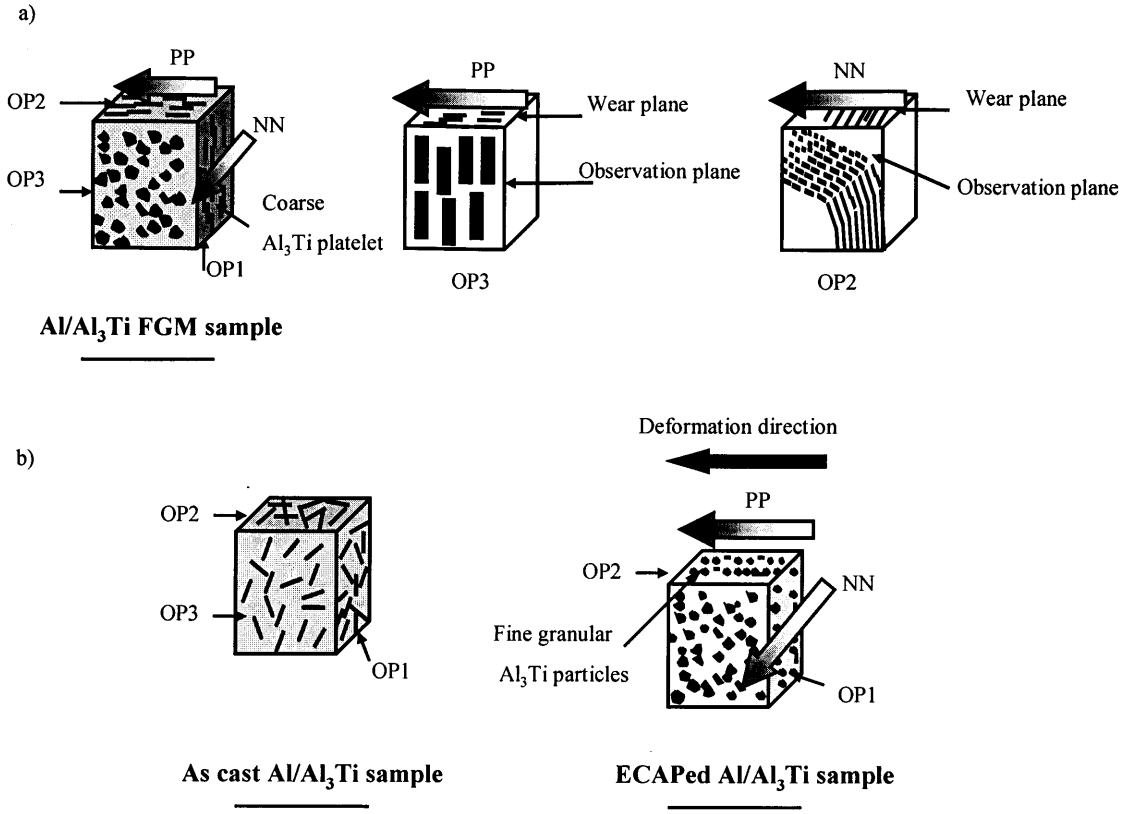


**Fig. 3.9. Schematic illustration of a) Al-$Al_3Ti$ FGM, b) ECAPed Al-$Al_3Ti$ composite and the description of wear test directions.**

With the above in mind, it is concluded that there are two main factors influence the anisotropy in the ECAPed Al-$Al_3Ti$ samples: the particles shape (coarse platelet/fine granular) and the particles alignment to a certain direction. Figure 3.10 (a) and (b) shows the relationship between the weight loss and the orientation parameter in the parallel and normal wear test directions, respectively. It is observed that increasing $f_p$ up to (~ 0.4) resulted in increased weight loss in both of PP and NN directions. However, the weight loss value decreased with further increase of the orientation parameter. This is because of the associated decrease in the particles size and aspect ratio with increasing the number of ECAP passes as shown in Fig.3.3.

a)

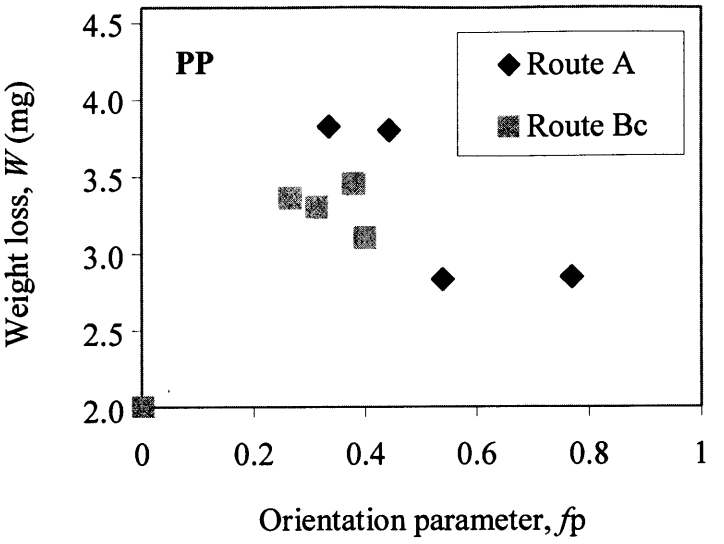


b)

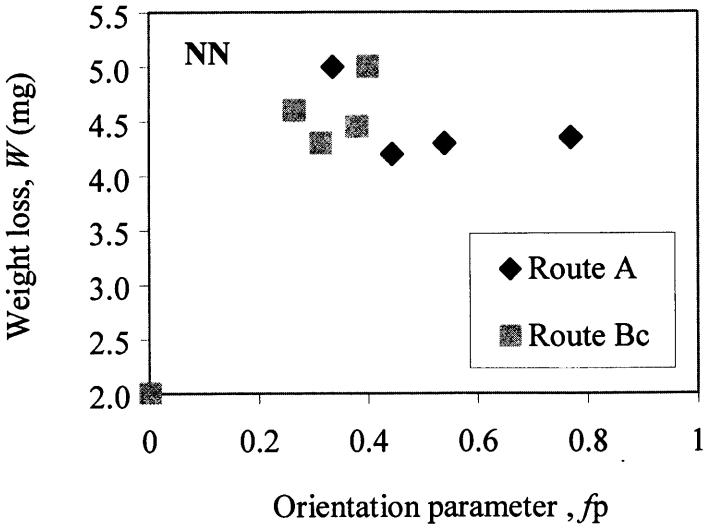


**Fig. 3.10. Weight loss of ECAPed Al-$Al_3Ti$ samples in a) PP and b) NN directions versus the particles orientation parameter.**

In order to understand the combined effect of both the orientation parameter and the particles size on the degree of anisotropy, Fig. 3.11 shows the calculated anisotropy (defined as weight loss of NN/PP) as a function of number of ECAP passes. From this figure, it is evident that the anisotropy increases with increasing the deformation up to 6 passes and hence increasing the particles alignment to the deformation direction. Upon further deformation, the anisotropy of the Al-$Al_3Ti$ samples decreased at 8 passes of ECAP using route A and route $B_C$. Though, the significant increase of $f_p$ value from 6 to 8 passes using route A which resulted in a banded structure, as shown in Fig. 3.2(b), was expected to increase the wear anisotropy. However, the smaller size and the lower aspect ratio of the $Al_3Ti$ particles observed at 8 passes A limited the effect of increasing $f_p$ on the anisotropy of the ECAPed samples. Therefore, the samples did not show larger anisotropy at 8 passes of ECAP.

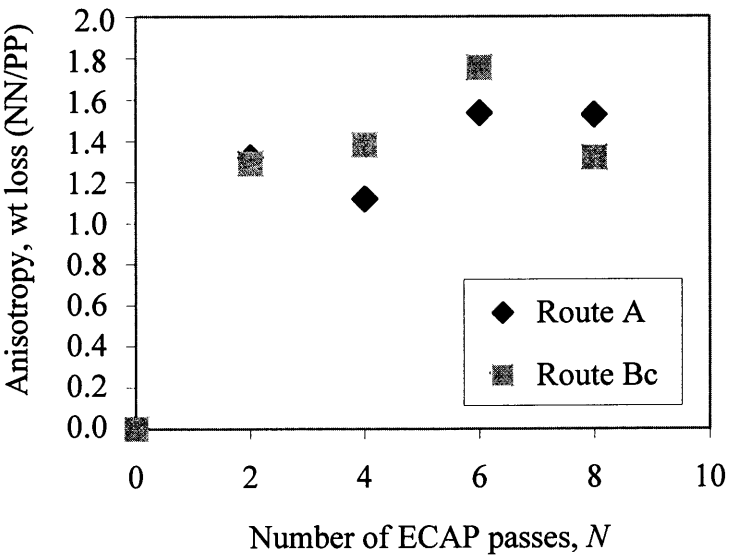


**Fig. 3.11. Variation of wear anisotropy of ECAPed Al-$Al_3Ti$ samples with number of ECAP passes.**

## 3.4. Conclusions

Based on the previous discussion, ECAP as one of SPD processes can alter the shape of the platelet $Al_3Ti$ particles and fragment it to very small sized granular particles. In addition, deformation by ECAP limits the anisotropy of the wear property in the Al-$Al_3Ti$ composite containing platelet particles regardless of the ECAP processing route.

## References:

[1] Zhang Z, Hosoda S, Kim I-S, Watanabe Y. Mater. Sci. Eng. A, 425 (2006) 55.

[2] Furuno K, Akamatsu H, Oh-ishi K, Furukawa M, Horita Z, Langdon T.G. Acta Mater., 52 (2004) 2497.

[3] Furukawa M, Horita Z, Langdon T.G. In, Chandra, T., Wanderka, N., Reimers, W. and Lonescu, M. (eds.) THERMEC. Switzerland, Trans Tech, 1946-195 (2009).

[4] Watanabe Y, Sequeira P.D, Sitdikov O, Sato H, Zhang Z, Kim I-S. Mater. Sci. Forum, 561-565 (2007) 251.

[5] Watanabe Y, Sato R, Matsuda K, Fukui Y. Sci. Eng. Comp. Mater., 11 (2004) 185.

[6] Sato H, Watanabe Y. Mater. Sci. Forum, 561-565 (2007) 659.

[7] Sequeira P.D, Ph.D Thesis, Nagoya Institute of technology, (2006).

[8] Nakashima K, Horita Z, Nemoto M, Langdon T.G. Acta Mater., 46 (1998)1589.

[9] Watanabe Y, Eryu H, Matsuura K. Acta Mater. 49 (2001) 775.

[10] Valiev R.Z, Islamgaliev R.K, Kuzmina N.F, Li Y, Langdon T.G. Scripta Mater., 40 (1999) 117.

[11] McGee S.H. , McCullough R. L. J. Appl. Phys., 55(1984) 1394.

[12] Watanabe Y. J. Compos. Mater., 36 (2002) 915.

[13] Furukawa M, Iwahashi Y, Horita Z, Nemoto M, Langdon T.G. Mater. Sci. Eng. A, 257 (1998) 328.

[14] Watanabe Y, Yamanaka N, Fukui Y. Metall. Mater. Trans. A, 30A (1999) 3253.

[15] Sato H, Murase T, Fujii T, Onaka S, Watanabe Y, Kato M. Acta Mater., 56 (2008) 4549.

[16] Valiev R.Z, Langdon T.G. Rev. Adv. Mater. Sci., 13 (2006) 15.

[17] Alpas AT, Zhang J. Met. Mater. Trans. A, 25A (1994) 969.

[18] Wu J.M, Li Z.Z. Wear, 244 (2000)147.

[19] Wu N.Q, Wang G.X, Li Z.Z, Wu J.M , Chen J.W. Wear, 203-204 (1997) 155.

# Chapter 4
# Mechanical Properties of Al-$Al_3Zr$ Functionally Graded Materials Fabricated by Centrifugal Solid-Particle Method

## 4.1. Introduction

In chapter 1, the methods by which functionally graded materials (FGMs) can be produced were explained. A special attention was given to the centrifugal method (CM) as the favored technique to fabricate the alloys wherein the intermetallics compound has a higher density than the matrix [1-7]. The selective reinforcement of the component surface obtained by CM results in a higher wear resistance in the surface while maintaining high bulk toughness as reported by Fukui and Watanabe [8, 9].

In section 1.2.2, the works by Watanabe *et al.* [10-12] on Al-$Al_3Ti$ FGMs including $Al_3Ti$ platelet particles using centrifugal solid-particle method (CSPM) were discussed. Effect of the platelet shape of $Al_3Ti$ particles and its oriented distribution on the wear anisotropy in the fabricated FGMs rings were also explained [13-16].

Comparing to Al-$Al_3Ti$ system, the microstructure of Al-$Al_3Zr$ FGMs observed in the reported work [17] leads us to expect anisotropy in their wear property as well. However, the direct relationship between the $Al_3Zr$ platelet particles orientation and the wear anisotropy in Al-$Al_3Zr$ FGMs has not been yet investigated. In the current study, Al-$Al_3Zr$ FGMs were fabricated by CSPM and the anisotropy of the wear property of FGMs samples has been investigated. A strong dependency of the wear anisotropy on the $Al_3Zr$ platelet particles orientation has been observed. In addition, the samples worn surface morphology was different when the wear test was performed in different directions. Studying both of the worn surface morphology and the sub-worn surface layer showed that plastic deformation induced by wear was the main mechanism during the wear process of Al-$Al_3Zr$ FGMs samples.

## 4.2. Experimental Procedure

### 4.2.1. Fabrication of Al-$Al_3Zr$ FGMs samples

A set of experiments was performed using a horizontal type centrifugal casting machine shown in Fig. 4.1. Since the centrifugal force affects the particles distribution and their orientation in the prepared samples as described by Sequeira *et al.* [17], Al-5 mass% Zr (Al-7 vol% $Al_3Zr$) FGMs were produced under different centrifugal force magnitudes of $G$= 30, 60 and 120 (units of gravity). Generally, fabrication of FGMs by the centrifugal method is classified into two categories based on the processing temperature [18-23] as previously discussed in section 1.2.2. In the current experiments, since the processing temperature was fixed to be 925°C, which is located under the liquidus temperature of the master alloy as shown in Fig. 1.2, the fabrication method belongs to CSPM. The molten Al-Zr alloy was then poured into a spinning cylindrical mold preheated up to 650°C. After this, ring-shaped FGM samples of 90 mm outer diameter and 20 mm thickness were obtained.

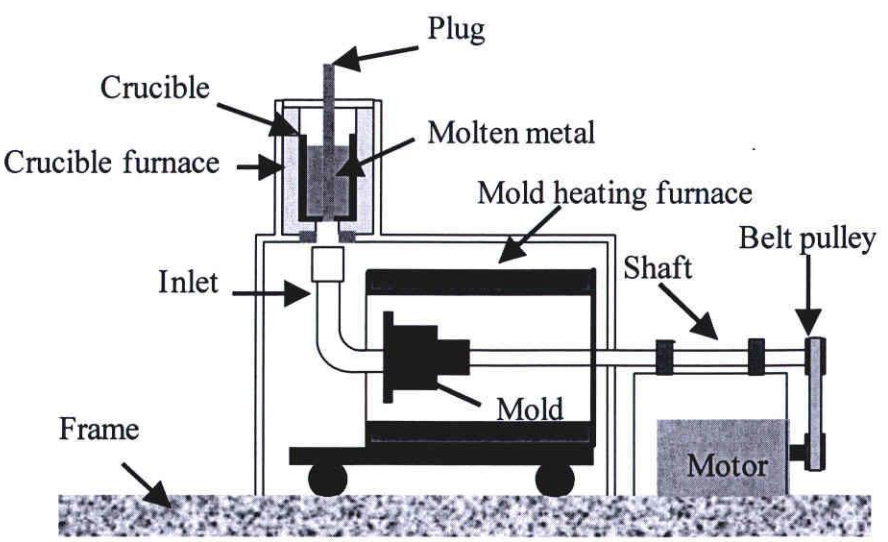


**Fig. 4.1. The horizontal type centrifugal casting machine used for the current experiments.**

The fabricated FGMs were cut parallel to the longitudinal direction and the centrifugal force direction (named plane OP2). The thickness of the samples was considered as normalized distance and divided into ten steps started from the outer surface of the ring (1.0) to the inner surface (0.0) as shown in Fig. 4.2. Microstructural observation for each position was performed by scanning electron microscope (SEM). The distribution of $Al_3Zr$ platelet particles and their orientation on plane OP2 have been investigated using SEM micrographs. The length of $Al_3Zr$ particles was then calculated using the linear intercept method. Volume fraction of the $Al_3Zr$ particles was determined by evaluating the area fraction of $Al_3Zr$ platelet particles at random positions using the SEM micrographs.

### 4.2.2. Mechanical properties evaluation

Vickers micro hardness on plane OP2 was measured at 0.49 N for 15 s from the outer to the inner surface of the rings with 0.1 step of the normalized distance, as illustrated in Fig. 4.2. A block-on-disc type wear test machine was used to investigate wide area of the fabricated Al-$Al_3Zr$ FGMs samples and to study the effect of large wear strain on the $Al_3Zr$ platelet particles fragmentation. In order to investigate the anisotropic wear property in Al-$Al_3Zr$ FGMs, the tests were carried out on plane OP2 in two directions, parallel and perpendicular to the $Al_3Zr$ platelets alignment named WP and WN, respectively. The wear test samples and directions are also presented in Fig. 4.2, the applied test conditions were 9.8 N load and 1m/s sliding speed. The worn surfaces and side surfaces of the worn specimens were observed by SEM. The sub worn surface layer was also studied through EDX observation of the Zr distribution in the layers next to the worn surface.

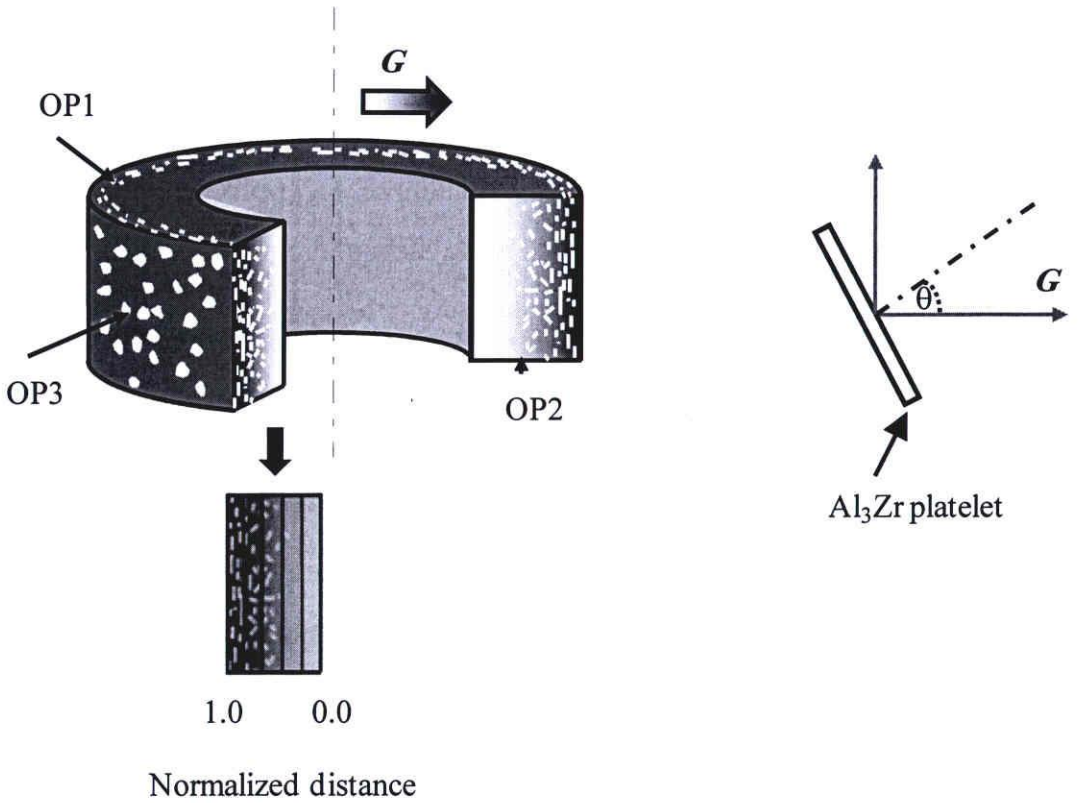


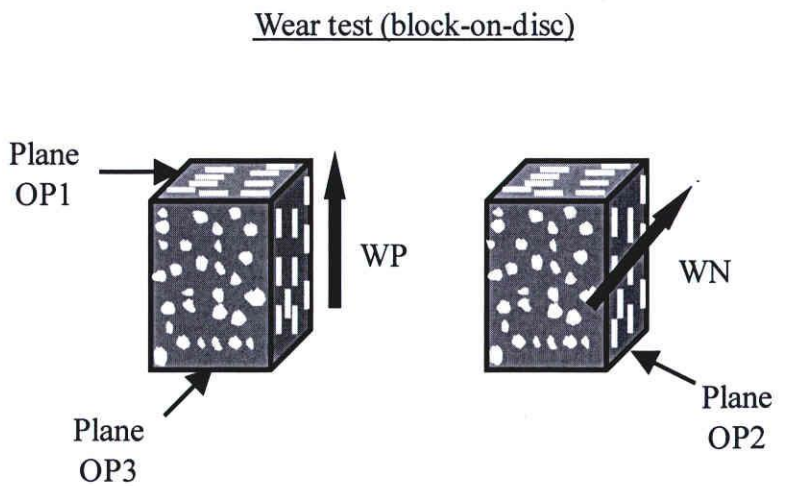


**Fig.4.2. Schematic illustration of the fabricated FGMs rings and the samples cutting directions.**

## 4.3. Results and discussion

### 4.3.1. Microstructure of Al-$Al_3Zr$ FGMs

#### 4.3.1.1. *Volume fraction distribution of $Al_3Zr$ particles*

Figures 4.3 (a), (b) and (c) are SEM compositional images showing the microstructure of the outer and inner surfaces of Al-$Al_3Zr$ FGMs fabricated under $G$= 30, 60 and 120, respectively. The microstructures of the outer surfaces present the large amount of $Al_3Zr$ platelet particles arranged normal to the centrifugal force direction. From this figure, it is clear that $Al_3Zr$ particles in Al-$Al_3Zr$ FGMs fabricated at relatively lower centrifugal force were distributed gently from the outer to the interior of the intermetallics rich area as shown in Fig. 4.3 (a). Next to this particles rich area, very fine $Al_3Zr$ particles were present in the inner surface of the FGMs as shown in Fig. 4.3 (a). On the other hand, increasing the centrifugal force resulted in a steep particles distribution and decreased thickness of the intermetallics rich area accordingly, Fig. 4.3 (c). Figures 4.4 (a) and (b) present the volume fraction and orientation distribution of the $Al_3Zr$ platelet particles in the fabricated FGMs. The observed decrease in the particles volume fraction from the outer to the inner part of the ring, Fig. 4.4 (a), can be owed to the gradual absence of the centrifugal force towards the ring inner surface.

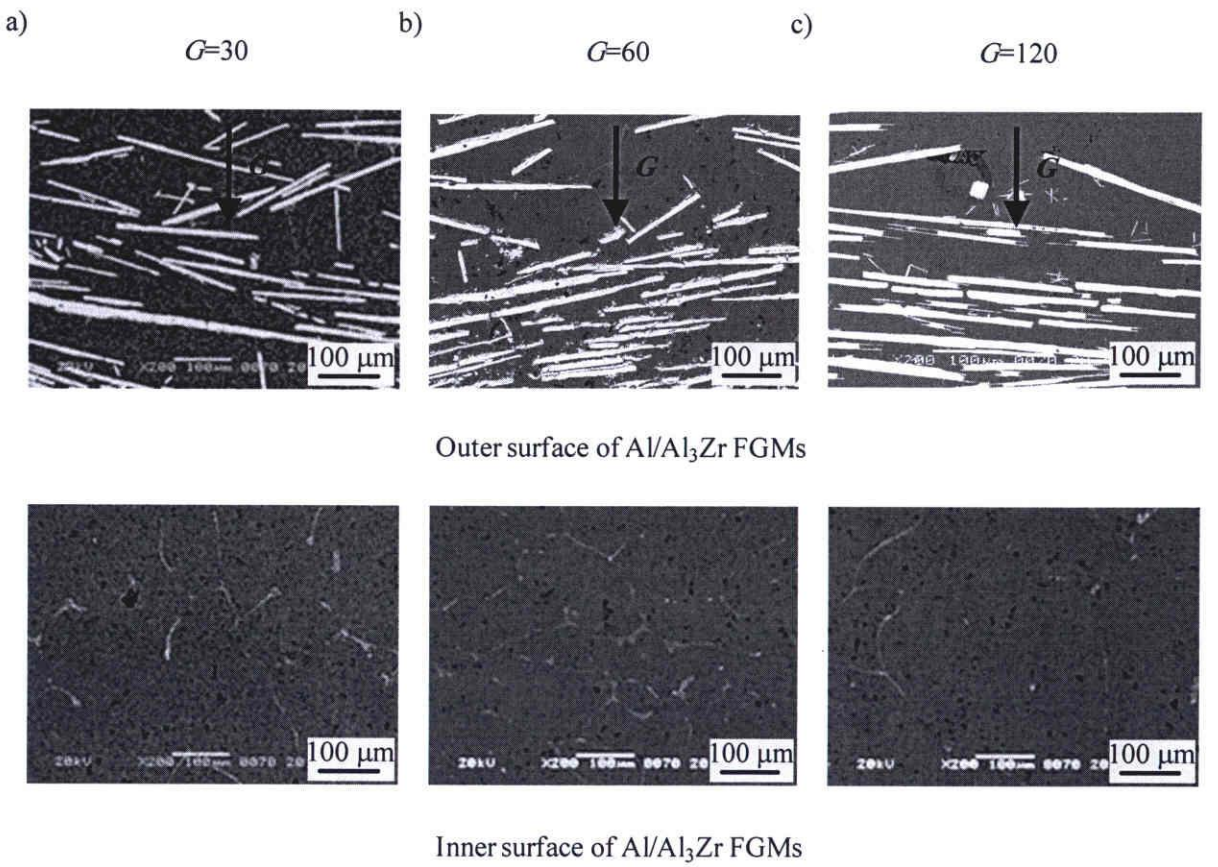


**Fig. 4.3. SEM micrographs using compositional mode of the outer and inner surfaces of the prepared Al-$Al_3Zr$ FGM samples.**

a)

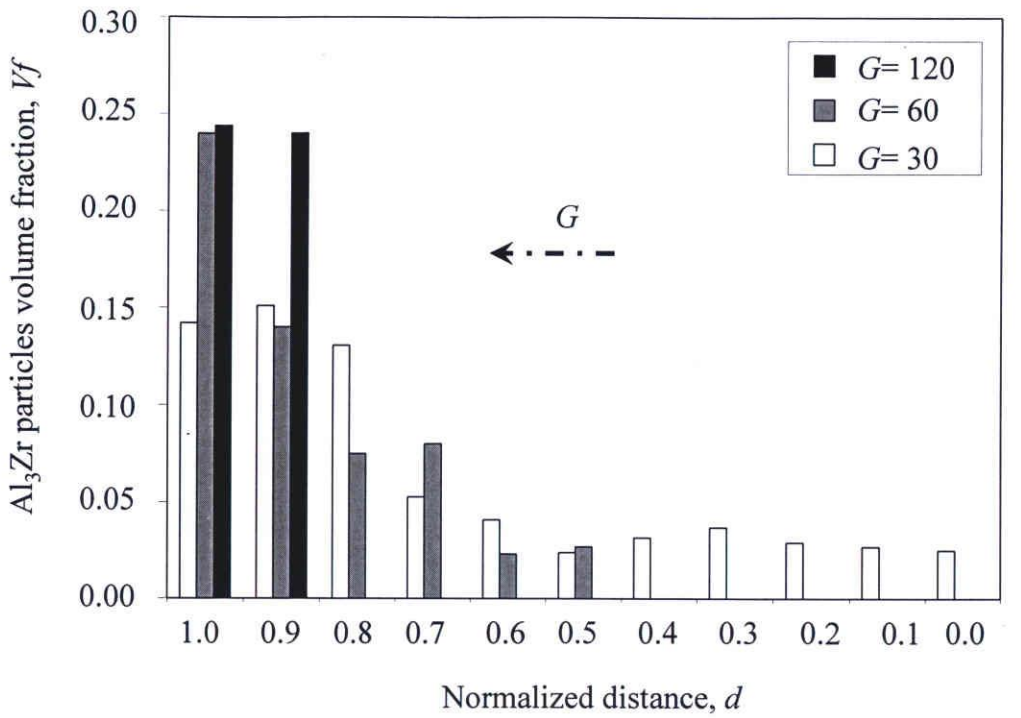


b)

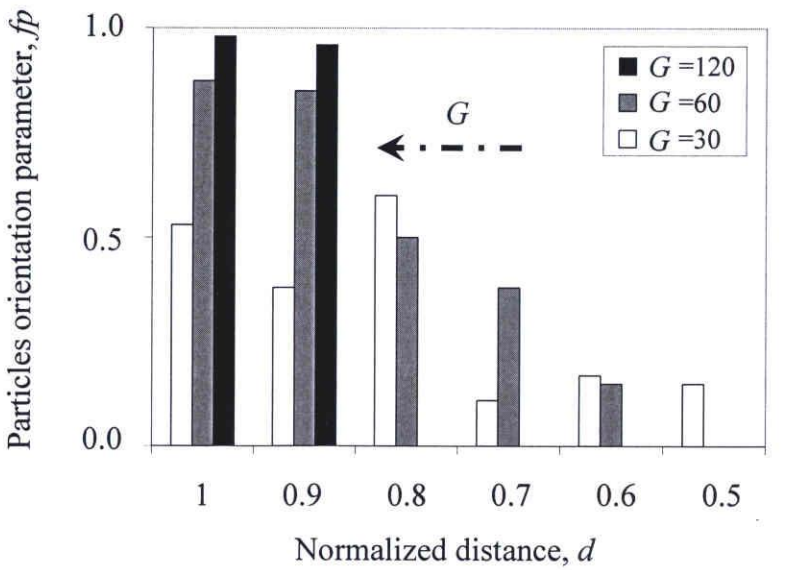


**Fig.4.4. Quantitative measurements of a) $Al_3Zr$ volume fraction distribution and b) orientation parameter, *fp* of the fabricated FGMs.**

#### 4.3.1.2. *Orientation of $Al_3Zr$ Particles*

The particles orientation is an important factor to consider when studying the wear property of the materials containing platelet particles [9]. Therefore, $Al_3Zr$ platelet particles alignment in the current study was investigated by calculating the orientation parameter, $f_p$ for each Al-$Al_3Zr$ FGMs sample. Considering the angle between the perpendicular to the platelet and the centrifugal force direction, $\theta$, as illustrated in Fig. 4.2, the $f_p$ could be calculated from the reported equation (2-1) [24-26] in 2.3.1. In case of Al-$Al_3Zr$ FGMs, $f_p$ value ranges from 0.0 for a random distribution to a maximum of 1.0 for perfect alignment of $Al_3Zr$ platelet particles normal to the centrifugal force direction. The $f_p$ values for the fabricated FGMs were plotted in Fig. 4.4(b).

From Fig. 4.4(b), it is seen that $Al_3Zr$ platelets in the interior surface are randomly distributed while the outer surface platelet particles have a good alignment distribution with their planes normal to the centrifugal force direction. Thus both of the orientation of $Al_3Zr$ platelets and the particles volume fraction are gradually distributed in the Al-$Al_3Zr$ FGMs. Comparing the degree of particles alignment among the three FGM rings; it is observed that the FGMs shown in Fig. 4.3 (a) have the lowest $f_p$ value in the outer region. On the other hand, FGM presented in Fig. 4.3 (c), has the most oriented particles in the outer area of the FGM rings.

This decreasing trend of $Al_3Zr$ platelets orientation from the outer to the inner surface of the fabricated FGMs rings and the observed lower orientation at the samples cast at lower $G$ number occurred due to the effect of centrifugal force [27]. The centrifugal force affect the volume fraction distribution of the particles thus different positions in the fabricated FGMs have different volume fraction of $Al_3Zr$. As can be seen in Fig. 4.4(a), higher volume fraction of $Al_3Zr$ is observed in the outer region of the rings for all specimens. In addition, this particles volume fraction increased with increasing the applied centrifugal force. The observed distribution in orientation parameter is caused by the position dependencies of these factors as reported by Sequeira *et al.* [27] for Al-Ti FGMs. This gradual distribution of both the orientation parameter and the particles volume fraction in the Al-$Al_3Zr$ FGMs lead us to expect

the positional dependency of wear property in the fabricated FGMs and will be described in the following sections.

### 4.3.2. Hardness distribution of Al-$Al_3Zr$ FGMs

Since wear is the result of the accumulation of plastic deformation and measurement of hardness is usually carried out to evaluate the resistance to plastic deformation, the relationship between wear and hardness has been extensively studied [28]. For traditional materials, both theory and experiments showed that the wear resistance increases with the hardness [29]. In Al-$Al_3Zr$ FGMs, since the particles volume fraction is distributed in a gradual manner, the hardness value should also show similar gradient distribution. Therefore, this concept should be deeply considered.

In the current study, Vickers hardness was measured from the outer to the inner surfaces of the FGM samples and the results were presented in Fig. 4.5. As shown in this figure, the outer surface of the samples has high Hv values and then Hv decreased with the gradual absence of $Al_3Zr$ particles towards the inner part of the ring. The gentle decrease of the hardness was observed in the FGMs fabricated under relatively lower centrifugal force, while a steep gradient was remarked when the applied centrifugal force increased. It is clear that the dependency of hardness distribution on the centrifugal force comes from the $Al_3Zr$ particle distribution. This further supports the expected dependency of wear property on the position in the fabricated Al-$Al_3Zr$ FGMs.

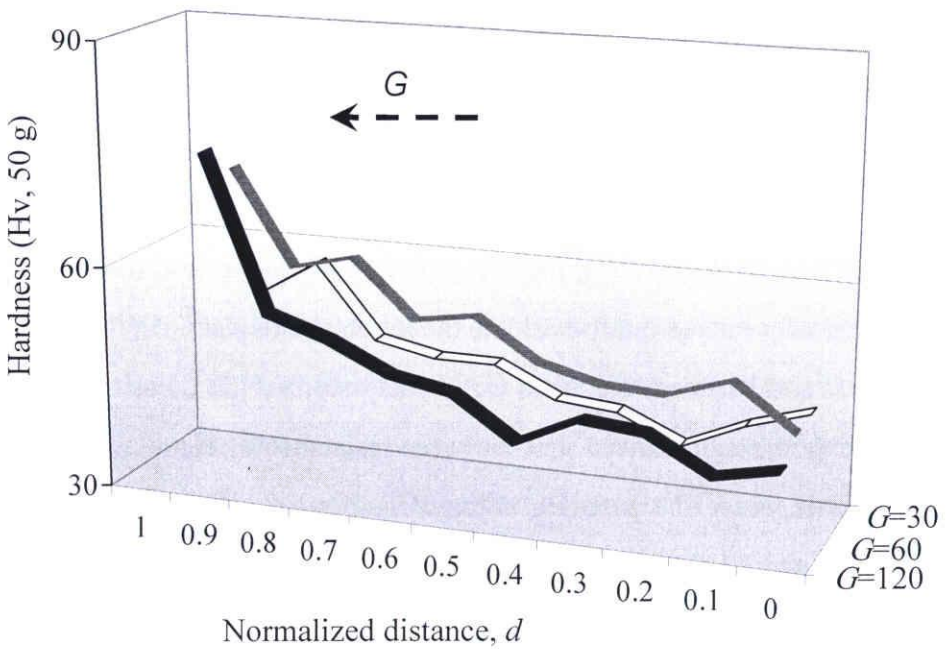


**Fig. 4.5. Hardness distributions along the FGM samples thickness.**

### 4.3.3. Wear behavior of Al-$Al_3Zr$ FGMs

#### *4.3.3.1. Wear anisotropy*

The block-on-disc wear test was carried out in order to show the influence of the gradient type on the wear resistance and wear anisotropy of the Al-$Al_3Zr$ FGMs. As previously mentioned the particles distribution gradient was steep in case of higher *G* number and became gentler when FGMs were processed under lower centrifugal force magnitudes. Figure 4.6 (a) shows the wear test results explained in volume loss for Al-$Al_3Zr$ FGMs fabricated at different *G* numbers. From this figure, it can be remarked that FGM prepared at lowest *G* number have the worst resistance among the fabricated samples. This is because the gentle gradient of particles distribution observed in the samples, in which the number of $Al_3Zr$ particles at tested region was decreased. Since the $Al_3Zr$ particles act as load supporting elements, decreasing their volume fraction allows the soft matrix to be involved in the wear process as described by Alpas and Zhang [30]. By comparison, the samples made under high *G* number achieved the

lowest volume loss when tested using block-on-disc wear type machine. This was expected considering the wear test samples cutting position, which was 5 mm apart from the outer surface of the samples where the FGMs cast under higher *G* number showed a remarkable occurrence of $Al_3Zr$ particles.

The anisotropy of the wear property in the fabricated rings could be identified through the difference in the wear volume values between the two test directions. Regarding the effect of testing at different orientations relative to the particles alignment, the results were in accordance with the reported work [14], where testing along WP direction showed more resistance to wear compared to the WN direction. In order to imagine the influence of wear direction on a group of aligned platelets, a simple schematic illustration of the process is shown in Fig. 4.6 (b). In case of testing along WP direction, the brittleness of the $Al_3Zr$ particles is very low and almost no damage occurs to the particles. On the other side, when the wear test is carried out along WN direction, damaged layers were observed indicating the brittleness of the $Al_3Zr$ platelets in the normal testing direction. The evidence is presented in Fig. 4.7, which shows the cross-section parallel to the sliding direction of Al-$Al_3Zr$ FGM sample cast at $G$=60 and tested in the WN direction. In this figure, damaged layers containing broken $Al_3Zr$ particles bended along the wear test direction can be observed.

Figures 4.8 (a) and (b) show the worn surface of the FGM samples tested in the WP and WN directions, respectively. Comparatively, there are significant differences in the worn surface morphology between WP and WN test directions. It can be found that the deformation level of the worn surface increased in case of normal testing direction, Fig. 4.8 (b). This is because of the size of laminar structures in WN direction is much larger than that of WP direction, which implies that the debris size resulted from WN is larger than that from WP [31]. In this way, the material on the contact surface was easier to deform under WN testing direction. This result is consistent to the increased volume loss in WN direction as shown in Fig. 4.6(a).

The variation of wear anisotropy with the particles orientation gradient in Al-$Al_3Ti$ FGMs was previously investigated by Watanabe *et al.* [9, 14]. According to their study, a greater anisotropy in the wear resistance of Al-$Al_3Ti$ FGMs is found for specimens with larger orientation parameter. Similar to their study, the anisotropy of the wear property of the current

Al-$Al_3Zr$ FGMs is diminished with decreasing the applied centrifugal force and thence decreasing the particles orientation. In order to quantitatively express the observed dependency of wear anisotropy on the particles orientation (presented in Fig. 4.4 (b)), the wear volume ratio (wear volume of direction WN/ wear volume of direction WP (shown in Fig. 4.6a)) was calculated and the results is presented in Fig. 4.9. As can be seen, the anisotropy of wear resistance can be emphasized with an increase in the orientation of the $Al_3Zr$ platelets.

a)

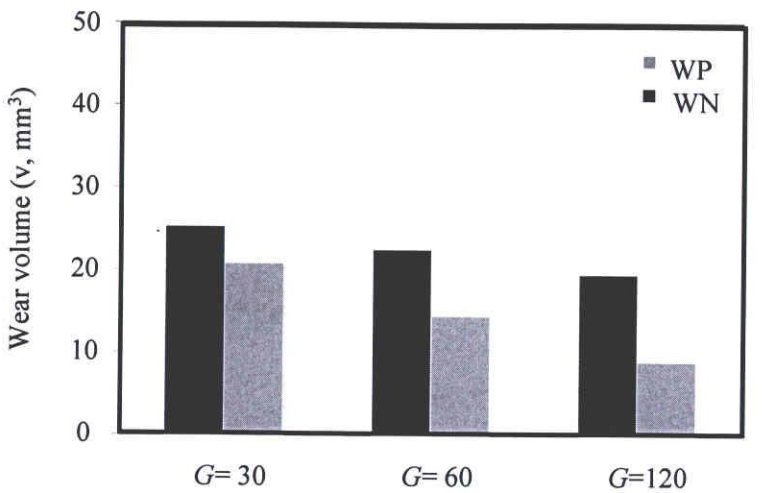


b)

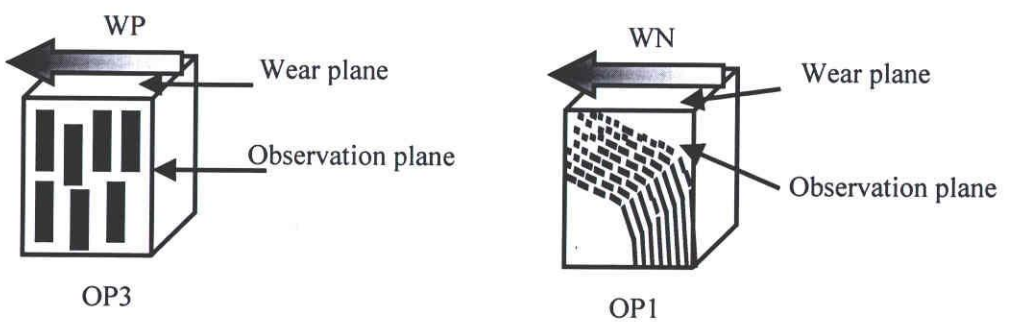


**Fig. 4.6. a) Block-on-disc wear test results b) Schematic illustration of the wear process in different directions relative to the particles alignment.**

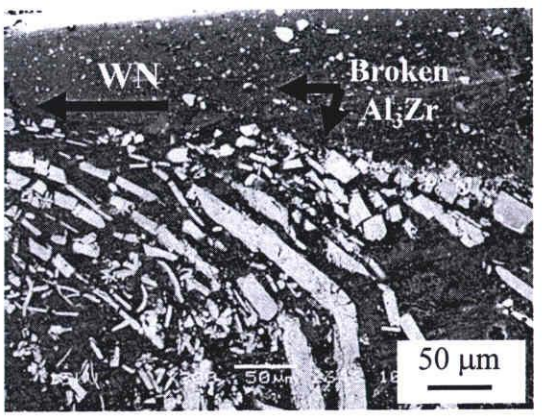


**Fig.4.7. SEM micrograph showing the cross-section parallel to WN of the samples prepared at *G*=60.**

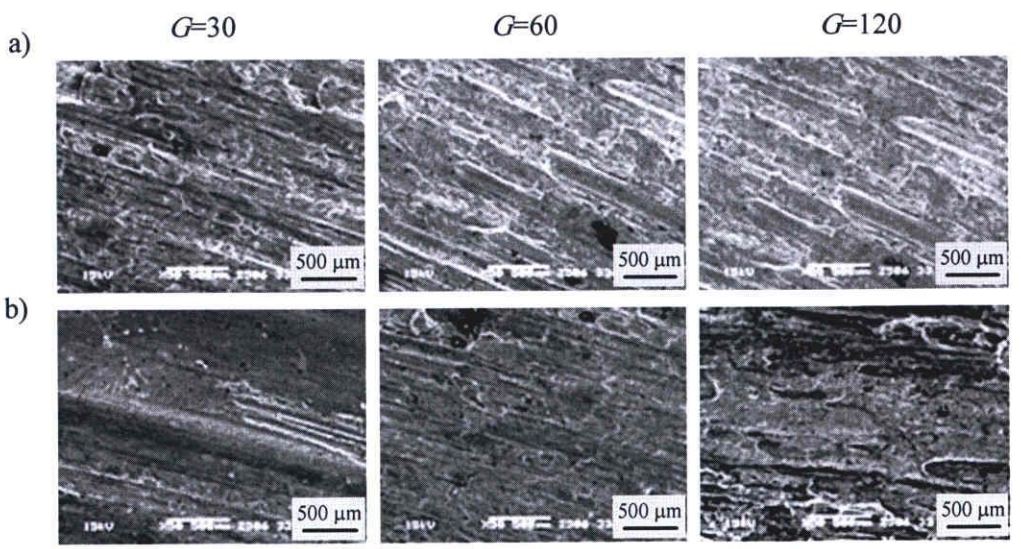


**Fig. 4.8. The Worn surface morphology of FGMs samples tested in a) WP direction and b) WN directions.**

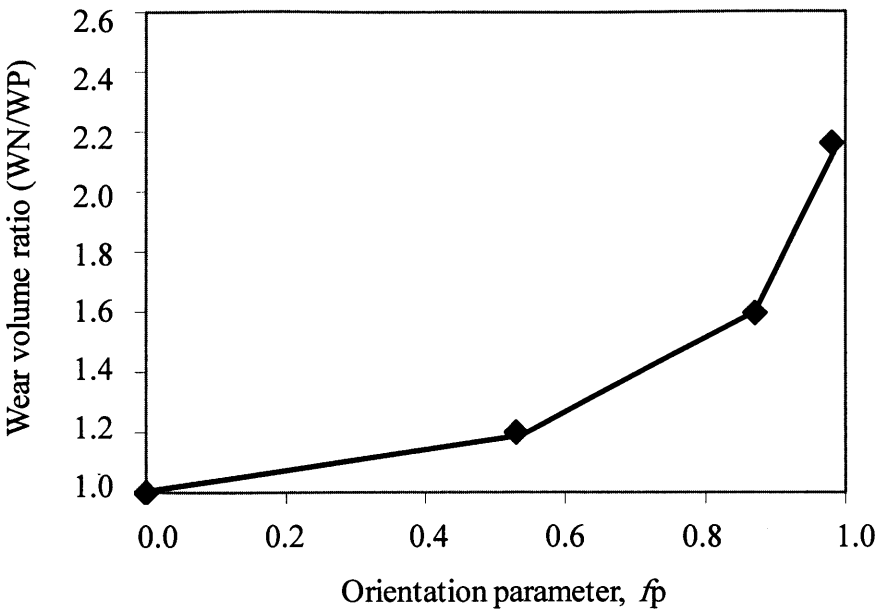


**Fig. 4.9. A plot of the wear volume ratio versus particles orientation parameter.**

### *4.3.3.2 Influence of severe wear strain on $Al_3Zr$ intermetallics*

It has been reported by Li and Tandon [32] that severe plastic strain near a worn surface is produced by sliding wear, especially in unlubricated states. This large plastic strain can alter both of the structure and the chemical composition of the sub-worn surface layer as Watanabe *et al.* [14] observed earlier. The formation of this wear-induced layer during the wear test was further investigated by Watanabe *et al.* [33] in their work on Al-$Al_3Ti$ FGMs containing brittle $Al_3Ti$ platelet particles. They have found that this layer contains Al-Ti supersaturated solid solution without the presence of $Al_3Ti$ phase and is formed very near to the worn surface during the abrasive wear. Sato *et al.* [34] have recently reported that this wear-induced layer forms due to the heavy shear deformation of the matrix, followed by fragmentation of the $Al_3Ti$ particles and finally the dissolution of some of those fine particles into the Al matrix. In the current Al-$Al_3Zr$ FGM samples, this layer has also been remarked. In addition, the occurrence of this layer was always observed wherever the severe wear cracks were present. Since the samples tested perpendicular to the platelets alignment showed lower resistance to wear, as shown in Fig.

4.6, the wear-induced layer was more identified. Moreover, the thickness of this layer in WN tested samples was relatively larger than that of WP testing direction. The best example of these samples was the one cast under centrifugal force magnitude of $G$=60, where many wear induced cracks were observed, as presented by black arrows in Figs. 4.10 (a) and (b). This in its turn confirms the brittleness of $Al_3Zr$ particles groups when tested normal to their alignment using block on disc wear test. As a result, larger anisotropy could be remarked compared to the parallel testing direction.

The Zr distribution in the wear induced layer and the following layers is shown in Fig. 4.10(c). From this Zr distribution map, it can be seen that Zr in the wear-induced layer was not condensed in particles but dispersed uniformly in the matrix. From the EDX analysis, presented in Fig. 4.10(d) for the subsurface layer and the following layer, pointed A and B respectively in Fig. 4.10(b), the composition of Zr at the supersaturated layer was analyzed to be roughly 9 mass % and this percent decreased in the following layers. However, this percent exceed the solubility limit of Zr in Al which is ~ 0.28 mass% at 660.45 °C [35]. This further confirms the formation of the Al-Zr supersaturated solid solution without the presence of $Al_3Zr$ particle.

With the above results in mind, both of the deformed sub-worn surface layer and the laminar structure of the worn surface shown in (section. 3.2.1) suggest that plastic deformation induced wear is the dominant wear mechanism for all of the FGM samples regardless of the test direction. The sub-wear regime is believed to be the abrasive wear. This is because of the presence of some detached $Al_3Zr$ particles on the samples worn surface, as observed in Fig. 4.8, which are characteristics of abrasive wear as described by Wu and Li [3].

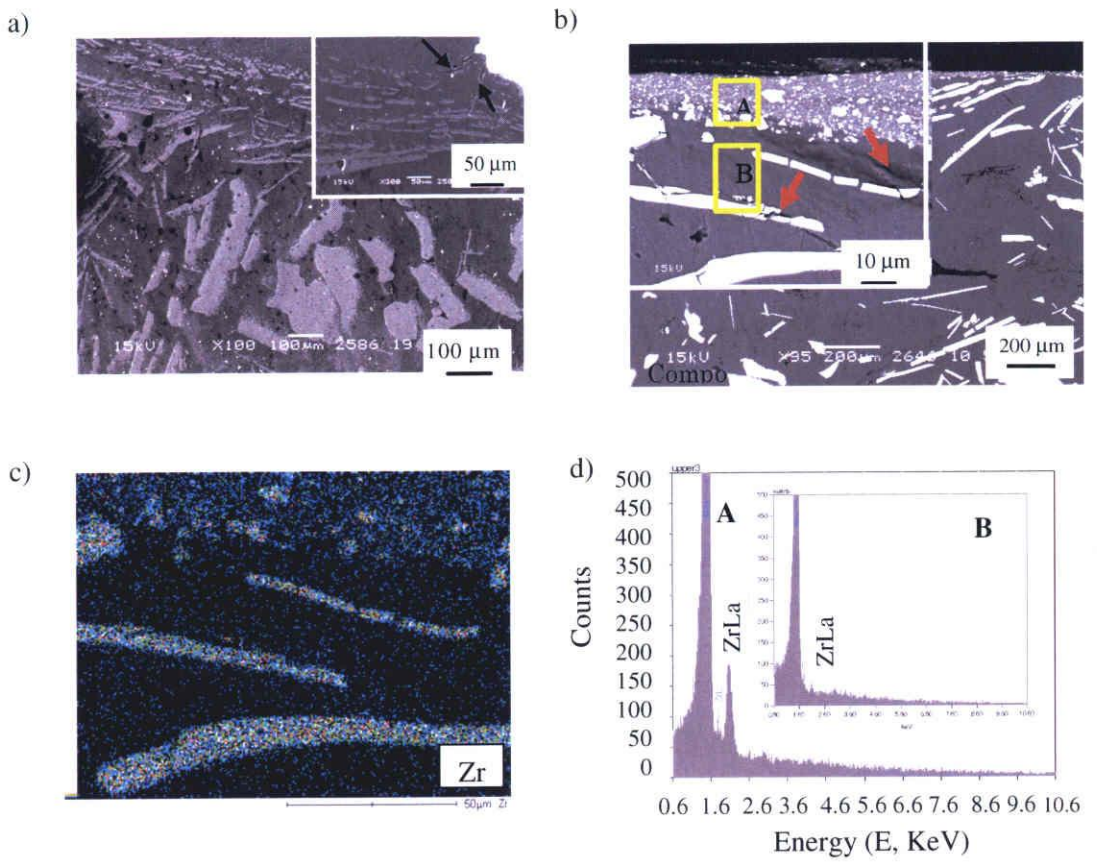


**Fig. 4.10. a) SEI micrograph, b) compositional image of the surface parallel to the worn surface of *G*=60 samples tested normal to the particles alignment, c) Zr map and d) EDS analysis of the layers next to the worn surface.**

## 4.4. Conclusions

Microstructural observation of the fabricated Al-$Al_3Zr$ FGMs showed that the platelet $Al_3Zr$ intermetallics in the outer regions were almost oriented normal to the applied centrifugal force direction and their degree of orientation along with their volume fraction decreases towards the inner part of the ring. These Al-$Al_3Zr$ FGMs showed different resistance to wear, which depends on the test direction relative to the particles alignment in the specified position. An enhanced wear resistance can be achieved in the Al-$Al_3Zr$ FGMs by controlling the distribution of both the orientation and the volume fraction of $Al_3Zr$ particles. A subsurface layer contains Al-Zr supersaturated solid solution without the presence of $Al_3Zr$ phase is

formed very near to the worn surface during block-on-disc wear test of the fabricated FGMs. This layer was more identified when the tests were performed perpendicular to the $Al_3Zr$ platelet particles alignment. The dominant wear mechanism is believed to be the plastic deformation induced wear. The abrasive wear was coexisted as sub-wear regime during the wear testing of FGM samples.

## References:

[1] Fukui Y. JSME Int. J. Series III, 34 (1991) 144.

[2] Ogawa T, Watanabe Y, Sato H, Kim I.S, Fukui Y. Composites Part A, 37A (2006) 2194.

[3] Wu J.M, Li Z.Z. Wear, 244 (2000) 147.

[4] Yamaguchi M, Inui H. $Al_3Ti$ and its L1 variations. In: Westbrook JH, Fleischer RL, editors. Structural applications of intermetallics compounds. 1995. New York: John Wiley, p. 151.

[5] Watanabe Y, Fukui Y. Recent Res. Devel. Metall. Mater. Sci., 4 (2000) 51.

[6] Sequeira P.D, Watanabe Y, Rocha L.A. Mater. Sci. Forum, 492 (2005) 609.

[7] Watanabe Y, Fukui Y. Aluminum Trans., 2 (2000) 195.

[8] Fukui Y, Watanabe Y. Metall. Mater. Trans. A, 27A (1996) 4145.

[9] Watanabe Y, Sato H, Fukui Y. J. Solid Mech. Mater. Eng., 2 (2008) 842.

[10] Watanabe Y, Kawamoto A, Matsuda K. Compos. Sci. Tech., 62 (2002) 881.

[11] Watanabe Y, Nakamura T. Intermetallics, 9 (2001) 33.

[12] Sequeira P.D, WatanabeY, Rocha L.A. Sol. Stat. Phen., 105 (2005) 415.

[13] Watanabe Y, Yamanaka N, Fukui Y. Metall. Mater. Trans. A, 30A (1999) 3253.

[14] Watanabe Y, Eryu H, Fukui Y. Ceramic Trans., 114 (2001) 675.

[15] Watanabe Y, Yamanaka N, Fukui Y. Z. Metallkd., 88 (1997) 717.

[16] Watanabe Y, Eryu H, Matsuura K. Acta Mater., 49 (2001) 775.

[17] Sequeira P.D, Watanabe Y, Rocha L.A. Mater. Sci. Forum, 492 (2005) 609.

[18] Watanabe Y, Fukui Y. Formatex Microscopy Book Series, 2 (2004) 189.

[19] Salim Z.M, Yamanaka N, Watanabe Y, Fukui Y, Nunomura S. Proceedings of the 2nd pacific Rim International Conference on Advanced Materials and Processing (PRICM-2) Adv

Mater Process, 2 (1995) 1739.

[20] Fukui Y, Takashima K, Ponton C.B. J. Mater. Sci., 29 (1994) 2281.

[21] Watanabe Y, Sato H, Matsuda R, Fukui Y. Sci. Eng. Compos. Mater., 11 (2004) 185.

[22] Fukui Y, Yamanaka N, Enokida Y. Composites part B., 28B (1997) 37.

[23] Watanabe Y, Oike S. Acta Mater., 53 (2005) 1631.

[24] McGee S.H, McCullough R.L. J. Appl. Phys., 55 (1984) 1394.

[25] Gonzalez L.M, Cumbrera F.L, Sanchez-Bajo F, Pajares A. Acta Metal. Mater., 42 (1994) 689.

[26] Watanabe Y. J. Compos. Mater., 36 (2002) 915.

[27] Sequeira P.D, WatanabeY, Eryu, H, Yamamoto T, Matsuura K. ASME Trans., 129 (2007) 304.

[28] Qian L, Xiao X. Appl. Phys. Letters, 84 (2004) 1076.

[29] Bhushan B, 2001. Modern Tribology Handbook (Chemical Ruther, Boca Raton, FL). 1, p. 273.

[30] Alpas A.T, Zhang J. Met. Mater. Trans. A, 25A (1994) 969.

[31] Tijun C, Jian L, Yuan H. Res&Dev., 6 (2009) 319.

[32] Li X.Y, Tandon K.N. Acta Mater., 44 (1996) 3611.

[33] Watanabe Y, Yokoyama K, Hosoda H. Mater. Sci. Forum, 396-402 (2002) 1467.

[34] Sato H, Murase T, Fujii T, Onaka S, Watanabe Y, Kato M. Acta Mater., 56 (2008) 4549.

[35] Yamashita K, Sato A, Watanabe Y, Yamanaka N, Fukui Y. International Symposia on Advanced Materials and Technology for the 21 st Century. Hawaii, Abstracts p. 6.